POLITECNICO DI TORINO
In collaborazione con l’università tecnica TU-Delft

Corso di Laurea Magistrale
in Ingegneria Aerospaziale

Tesi di Laurea Magistrale

Homogeneous internal damage detection in an epoxy-amine system through the use of the Continuous relaxation spectrum

Relatori
Prof. Santiago J. Garcìa Espallargas
Prof. Marco Sangermano

Candidato
Serena Pipolo

Luglio 2022

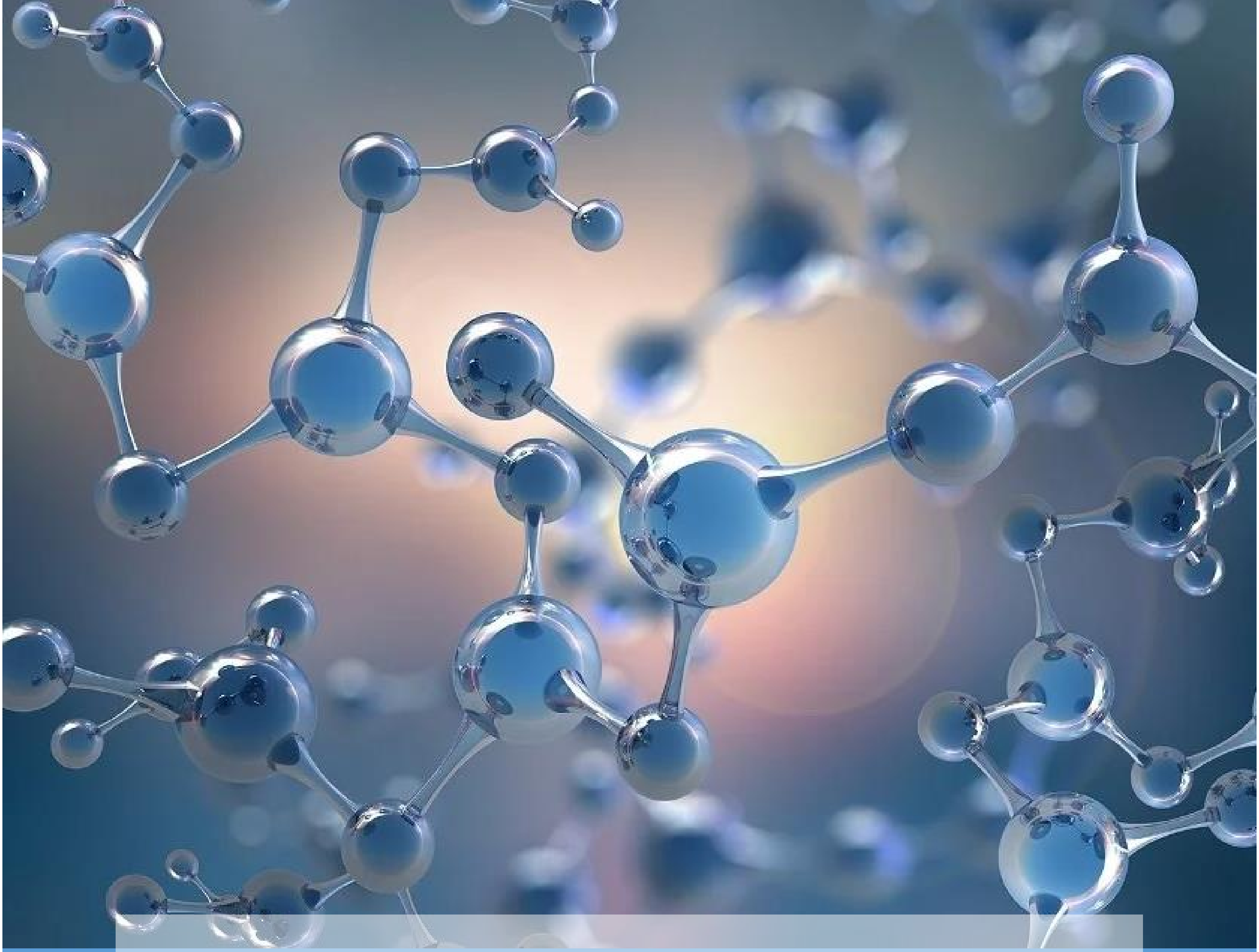

MSc thesis in Aerospace Engineering

Homogeneous-internal damage detection in an epoxy-amine system through the use of the continuous relaxation spectrum

Serena Pipolo

Politecnico di Torino

TU Delft

HOMOGENEOUS-INTERNAL DAMAGE DETECTION IN AN EPOXY-AMINE SYSTEM THROUGH THE USE OF THE CONTINUOUS RELAXATION RESPONSE

in partial fulfillment of the requirements for the degree of

Master of Science
in Aerospace Engineering

at Politecnico di Torino

by

Serena Pipolo

July 2022

Serena Pipolo: *Homogeneous-internal damage detection in an epoxy-amine system through the use of the continuous relaxation response* (2022)

The work in this thesis was made in the:

Novel aerospace materials research group

Department of Aerospace Structures and Materials
Faculty of Aerospace Engineering
Delft University of Technology in collaboration with Politecnico di Torino

Supervisors: Prof. Santiago J. García Espallargas
Prof. Marco Sangermano

ABSTRACT

In the last decades, a new class of materials has been developed and is being further improved nowadays: the class of self-healing materials. This category of bio-inspired materials is potentially capable of repairing structural or functional damage in different ways, increasing the material lifetime. Polymers are the most studied material class in the field.

For a better design of these materials, it would be of enormous importance to detect and quantify the invisible internal damage occurring in the samples, in order to value the healing efficiency before the ultimate failure. Nevertheless, most of the available scientific literature focuses on macroscopic and optically detectable damage.

Just recently a new technique was used to analyze damage degree and damage restoration, before the break, in a self-healing polymer network containing dynamic sulfur-sulfur bonds. Through the new protocol, the rheology data, acquired to build the polymer master curve, are used to get the continuous relaxation spectrum (CRS). The spectra obtained testing pristine and damaged specimens, before and after the healing, are compared, but from the results it is not clear the role played by time-dependent factors on curves variations.

In this work, in order to understand the technique ability to detect damage and exclude from results variation, the uncertainty due to experimental errors, and time-dependent effects, a non-healing epoxy-amine system is examined. The choice of the network allow reducing the number of variables affecting the dynamic response and so changes in spectra. The specimens are tested in both their pristine and damaged state and after a thermal treatment which emulate the healing triggering mechanism.

A major degree of scatter is observed in the pristine state spectra. Instead, the damage induction and the oven treatment, appear to reduce data variability. Samples heterogeneity and residual stresses from curing are found to be the most probable influence factors in CRS deviations in the pristine state, not allowing good comparisons with the damaged state.

The technique confirms itself to be a very sensitive instrument, able to capture the different states of stress within the samples. For this reason, a better knowledge about the samples network (chemistry, defects, cross-linking percentage) and/or trying to reduce the starting heterogeneity (e.g. with an oven treatment) would be necessary to really understand the curves shifting.

Also, it is not excluded that a different interpretation of the curve could lead to a more detailed phenomenal explanation.

SCOPO DELLA TESI E OUTLINE

Questo lavoro è stato realizzato in collaborazione con il gruppo di ricerca *Novel Aerospace Materials*, del dipartimento di Strutture e materiali per l'aerospazio dell' università TU-Delft.

Il suo scopo ultimo è lo sviluppo e la validazione di un protocollo sperimentale che consenta di individuare uno stato di danneggiamento, nella sua fase primordiale, all'interno di un network polimerico.

Lo sviluppo di tale tecnica di caratterizzazione ha come potenziale campo di applicazione lo studio dell'efficienza dei materiali self-healing. L'idea iniziale parte dal seguente presupposto: se è possibile individuare e quantificare uno stato di deformazione plastica all'interno di un campione, teoricamente, la stessa procedura può essere utilizzata per riconoscere il grado di riparazione in un materiale di tipo self-healing.

La tesi presenta la seguente struttura.

Nel capitolo 1 è presente una breve introduzione ai materiali self-healing e alle tecniche maggiormente utilizzate in letteratura, per studiare la capacità di autoriparazione.

Nel capitolo 2 verrà presentata la nuova procedura sperimentale per la descrizione della risposta dinamica dei materiali polimerici. Questa porta alla costruzione del *Continuous relaxation spectrum*, una funzione di distribuzione che segue l'andamento del modulo di rilassamento in funzione del tempo.

Attraverso il nuovo protocollo, si intende valutare lo stato di danneggiamento, prima dell' arrivo al punto di rottura, in un set di campioni epossi-amminici.

Il capitolo 3 illustra le fasi sperimentali: si parte dalla produzione dei campioni e dalla loro caratterizzazione termica e meccanica per poi passare alla descrizione del protocollo utilizzato per introdurre lo stato di danneggiamento e ottenere la funzione di distribuzione.

Nel capitolo 4 sono presentati i risultati dei test termici, meccanici e dinamo-meccanici.

Il capitolo 5 presenta la discussione dei risultati, le conclusioni e suggerimenti per eventuali test futuri.

RINGRAZIAMENTI

La scrittura dei ringraziamenti finali mi ha sempre terrorizzato. È difficile, se non impossibile, condensare in poche righe tutti gli anni trascorsi all'università, le esperienze vissute, le persone incontrate.

Quello che si può sicuramente dire è che solo alla fine ci si rende conto di quanto gli anni siano trascorsi in fretta e di quanto si è cambiati lungo il percorso.

Pezzi di te sono rimasti indietro, sulla strada, pezzi di qualcos'altro adesso fanno parte di te. Per quanto pensiamo di poter portare tutto quello che abbiamo raccolto con noi, qualcosa va inevitabilmente lasciata alle nostre spalle per fare spazio al nuovo. Persino sogni e speranze non sono più gli stessi: hanno ceduto il passo a pensieri più concreti che continuano a scontrarsi con l'idea futura di te che avevi da bambino.

Arrivare alla fine di un qualcosa è sempre difficile. La nostra natura ci costringe a tirare le somme, a pensare a tutto quello cui non avevamo pensato, avendolo rimandato a tempi futuri. Negli ultimi mesi mi sono spesso fermata a pensare a quale fosse lo scopo della vita, o almeno della mia, senza arrivare ad una precisa conclusione. Ho imparato che guardarti così dall'alto non è utile e può farti perdere la direzione. Per ora, mi consolo con l'idea che non sia ancora arrivato il mio tempo di saperlo.

Questi anni mi hanno lasciato molti ricordi, non tutti sempre belli, ma un'esistenza sempre felice, oltre che non esistere, perderebbe di significato. E più che le lezioni universitarie, le persone che ho avuto la fortuna di incontrare o che ho avuto la fortuna di avere accanto a me da molto più tempo, hanno determinato in parte la persona che sono oggi.

Credo, infatti, che le persone siano un' incredibile fonte di ispirazione: ho conosciuto il loro impegno, la meticolosità, la voglia di combattere ma anche il saper prendere la vita alla leggera, il non prendersi troppo sul serio, il saper mostrare e condividere le proprie emozioni, la volontà di migliorarsi ogni giorno, il saper essere cattivi quando ce n'è il bisogno, la loro curiosità... Sono lezioni che cercherò di portare con me e che avranno sempre il nome di qualcuno di loro.

Ma ora, senza tirarla per le lunghe, veniamo ai ringraziamenti.

Il primo grazie va sicuramente alla mia famiglia, per avermi sempre supportato e aver creduto in me (forse anche troppo). Grazie delle opportunità, non scontate, che mi avete consentito di avere.

Un grazie alle mie sorelle che, anche se a distanza, mi hanno sempre incluso nelle loro vite, più di quanto abbia fatto io.

Grazie ad Antonio per essere cresciuto insieme a me e per essermi vicino pur non essendo sempre semplice.

Grazie a Federica, Marinax2, Martina e Antonia, alle risate, ai bei momenti, al vino condiviso e al vostro supporto essenziale.

Grazie ai miei compagni di avventura Domenico, Leo, Lorenzo e Pietro, con voi questi anni non sono mai stati noiosi, grazie per il vostro affetto e per la fiducia nei miei confronti.

Grazie agli inquilini di Via Perosa (anche quelli acquisiti) non avrei potuto chiedere di meglio.

Grazie a Gaetano, Luca e a tutti gli altri amici incontrati a Torino per essere stati una seconda famiglia.

Grazie ad Andrea, Alessandro, Gianni e tutti gli amici di giù, mi perdonerete se non vi elenco tutti, sapete bene che l'affetto e il riconoscimento vanno ben oltre le parole.

Infine, ma non meno importanti, grazie ai prof Santiago e Marco per avermi guidato durante lo sviluppo di questa tesi e alla bellissima comunità di persone conosciute alla TUDelft. Grazie per avermi fatto sentire parte di voi durante la mia permanenza, per avermi arricchito condividendo con me curiosità sulle vostre culture e per avermi fatto crescere anche da un punto di vista scientifico.

Grazie ancora a tutti per aver fatto parte della mia vita, per aver condiviso con me solo qualche fermata o molto di più.

CONTENTS

LIST OF FIGURES

1 INTRODUCTION

The damage could be defined as the progressive physical process that brings a material to rupture. Different scale levels can be used to describe the mechanism of the damage: at the microscale level is the accumulation of micro stresses near the interfaces and the breaking of bonds, at the mesoscale, it is the initiation of the crack by the coalescence of microcracks or microvoids, at the macroscale, it is the growth of the crack [1].

Depending on the materials, damage may occur in different ways but in all cases, it directly influences the material elasticity and plasticity. The first, since the number of atomic bonds, strongly related to elasticity, decreases with damage, and the second, because the elementary area of resistance decreases with the number of bonds. In polymers, it is manifested at the elastic level by the breakage of bonds that exists between the long molecular chains and at the plastic level by the arrangement of molecules.

Of course, the presence of damage in the structures makes their lifetime shorter, since the mechanical properties are affected. Hence, in the last decades, many non-destructive methods for damage detection were developed. Their usage allows recognizing when the crack dimensions in a component reach a critical value, in order to substitute it before its failure.

In the last 20 years, another strategy has been studied, based on the biological concept of 'self-repairing', a new class of materials is being developed: the class of *self-healing materials*. This category of bio-inspired materials is potentially capable of repairing structural or functional damage in different ways, increasing material lifetime (Figure 1.1).

Today, polymers (and composites) are the material class most studied in the field. This may be due to the polymeric system's ease of functionalization and modification, or even the low temperatures required to induce mobility in the network and the large volume of mobile molecules in comparison to the volume of mobile atoms [2].

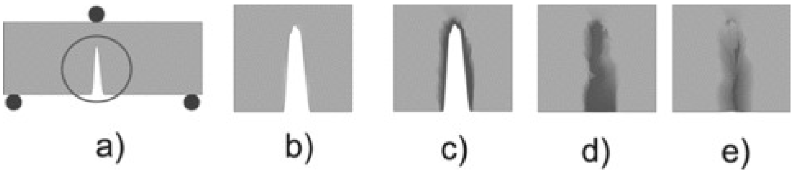

Figure 1.1: Macroscopic self-healing steps. [2]

Depending on the healing mechanism, self-healing polymeric materials can be divided into two main classes: extrinsic and intrinsic healing. The extrinsic type contains discrete entities filled by a healing agent (such as a liquid adhesive or solvent) that are released in the polymer, after a crack formation, if the discrete entities break. The healing agent will fill the gap and react with the surrounding molecules to heal the damage [3, 4, 5, 6].

The intrinsic healing mechanism is based on the re-establishment of bonds due to the incorporation of reversible bonds/reactions in the polymer networks (Figure 1.2). In this case, the healing mechanism is triggered by an external stimulus that brings temporary local network mobility necessary for filling the crack and reconnecting the reversible chemistries [7, 8, 9].

By the way for a better design of this material would be of enormous importance detecting and quantifying the damage occurring and then value the healing efficiency.

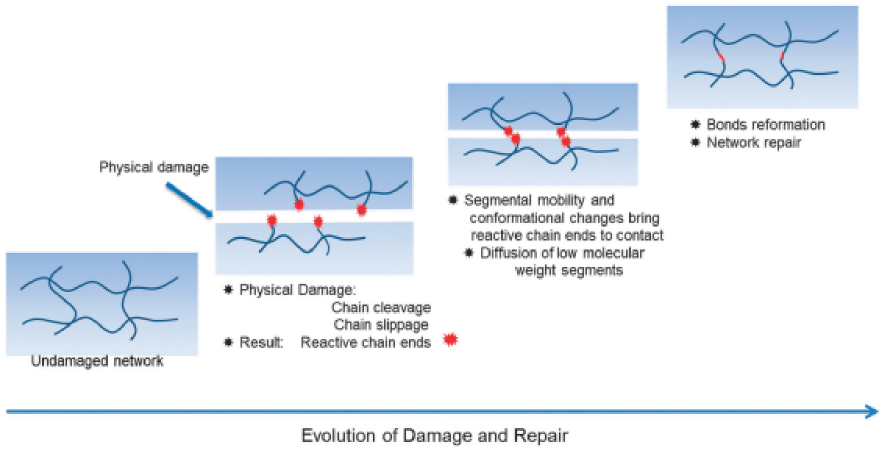

Figure 1.2: Ideal evolution of a damage-repair cycle in polymeric materials. [10]

Healing efficiency has been assessed mostly by tracking mechanical properties recovering, such as fracture, impact, or fatigue, at a macroscale level when the defects are easily visible.

The healing at the fracture site of a local destructive damage is one of the mostly studied type of self-reparation. After damaging the polymer until its complete failure, the two obtained halves are placed together and the activation of the healing mechanism is allowed under one or different external stimuli. The healed samples are then re-tested and the evolution of the mechanical properties is tracked [11, 12].

Macroscopic and optically detectable damage is important but just a few studies are present in the literature instead, about the healing of invisible internal damage. Deep knowledge of the early-stage damage restoration, would be necessary for practical applications of self-healing materials since the healing of damage before ultimate failure is their main aim.

One example is the study conducted by Post et al. [13] about the self-repair of mechanical properties of intrinsically self-healing polymer particulate composite after fatigue loading conditions. In his work, poly (ethylene-co-methacrylic acid) zinc ionomer/Fe3O4 nanoparticle composites were developed and subjected to different levels of fatigue loading. The healing mechanism was triggered by an alternating magnetic field.

Another work by Hernandez et al. [14] investigates healing after fatigue damage in an elastomer. The broadband dielectric spectroscopy (BDS) was used as a technique to monitor damage healing. Through the analysis of the dynamic relaxation has been possible to see the formation of a heterogeneous network structure at the healed interface and also, to observe both damage and healing inside the network by looking at the dielectric loss spectrum's frequencies shift. Indeed, the BDS allows describing polymer's mobility as a function of polymer architecture which is changing during the damage-healing steps.

Lately, another interesting technique has been used for the same purpose by Roth: *the continuous relaxation spectra* (CRS) [15].

This work investigated whether damage degree and damage restoration after plastic deformation in a self-healing epoxy-silane dual network, containing dynamic sulfur-sulfur bonds, can be identified via CRS.

By comparing the spectra, it was found that any level of plastic deformation induces changes in the energy curve compared to the pristine state. Moreover, after the healing step, the curve appears to be shifted towards longer relaxation times.

The shift was not present anymore after waiting one week as recovery time from the oven treatment.

Also, an epoxy non-healing system in its pristine state has been used as a reference sample and it was possible to observe the differences in the dynamic of the two network systems: the self-healing one shows a faster dynamic of the main relaxation peak.

Roth's research has already shown that the damage and healing bring changes in the relaxation spectrum but is important to acquire new data on a damaged simpler network system, in order to distinguish the contributions in the relaxation process of the permanent crosslinked part. Indeed, in literature, there is a lack of information about the relaxation response of crosslinked polymers.

In this research, an investigation about how damage and time-dependent factors affect the CRS is made, in order to understand and quantify the sensibility of the technique in capturing different equilibrium states of the polymer tested and confirm the technique's capability of detecting the damage with a certain degree of confidence in the results.

For this purpose, pristine and damaged state samples of an epoxy-amine system have been tested. The effects of a heating treatment are investigated, considering different cooling rates after the thermal treatment. Also, the time between the experimental steps is taken into account, as in Roth's research, it showed itself to be a key parameter.

2 THE CONTINUOUS RELAXATION SPECTRUM

Viscoelastic materials, such as polymers, can exhibit both viscous and elastic behavior and time represent a key parameter to determine which behavior prevails.

Viscoelasticity characterization is very important during the design of a new polymer to predict product performance and processing behavior. Indeed it affects the transmission, storage, and dissipation of force and energy. Moreover, variations in viscoelastic response as a function of loading duration or frequency can provide indications about micromechanical deformation, resilience mechanisms, and molecular structure [16].

The common way to study the viscoelasticity of an entangled polymer is by analyzing the rheological data provided by the storage and loss moduli plots versus the frequency or the temperature. The storage modulus relates to the material's ability to store energy elastically, while the loss modulus is related to the material's ability to dissipate stress through heat (Figure 2.1).

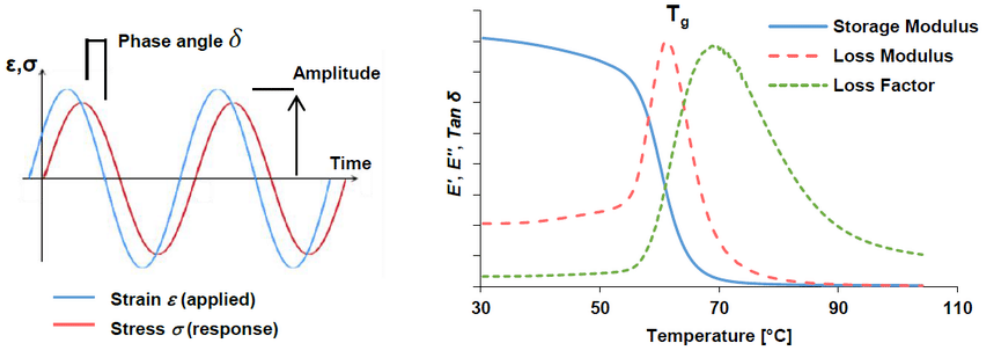

Figure 2.1: Example of a typical storage modulus, loss modulus, and loss factor plot. [17]

However, some features of particular interest are not well revealed by such representation of data [18]. Through the use of the continuous relaxation spectrum (CRS) these features can be revealed quite clearly.

The CRS physically represents an energy distribution function that shows the relaxation intensity (H) with the time (τ), as shown in Figure 2.2.

It could be considered as an idealized stress relaxation experiment wherein a polymeric sample, maintained at a constant reference temperature, is strained and then the relaxation response is observed [19, 20].

From an analytical point of view, several mechanical models can be used to obtain the necessary functions to build the relaxation curve. The most common is the infinite Maxwell model, which assumes an infinite parallel arrangement of Maxwell elements (spring and dashpot connected in series) [21].

The first studies published in the literature about the CRS, concern the rheological data analysis to obtain the best spectrum function to describe the relaxation behavior of a wide range of polymer materials.

In E. Kontou's research [22], dynamic mechanical data for a low-density polyethylene and for an epoxy resin based on amine cured DGEBA, have been used to fit the parameters of the CRS functions.

In Weese et al. work [23] the rheological data have been used to develop a nonlinear regularization method to overcome calculation issues since the determination of the relaxation spectrum is an ill-posed problem.

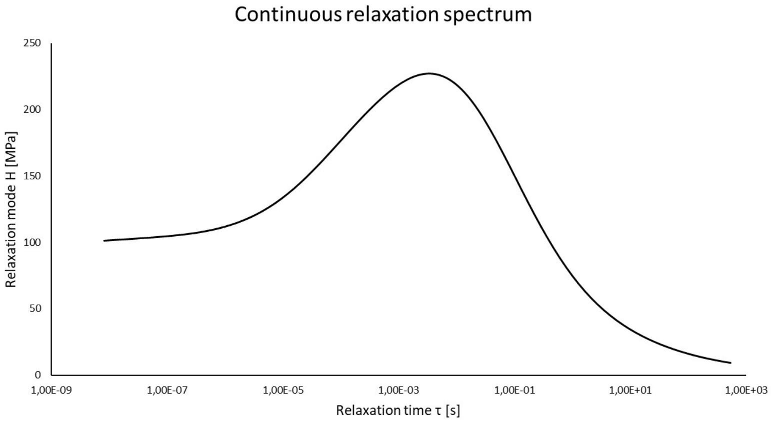

Figure 2.2: Continuous relaxation spectrum obtained for an epoxy-ancamine system.

Other works instead, made use of the potentiality of the spectra to find out interesting polymers properties not easily distinguishable from other characterization techniques.

Ankiewicz and co-workers [18] converted polyisoprene binary blends rheological data into the CRS model and it was easier to recognize the relaxation peaks due to the different polymer's features. The same procedure was followed for a polystyrene H-polymer. In this case, the characteristic power-law behaviors, at short relaxation time ($H \propto \tau^{-\frac{1}{2}}$) and at long relaxation time ($H \propto \tau^{-\frac{1}{4}}$), were clearly recognizable from the spectrum Figure 2.3a.

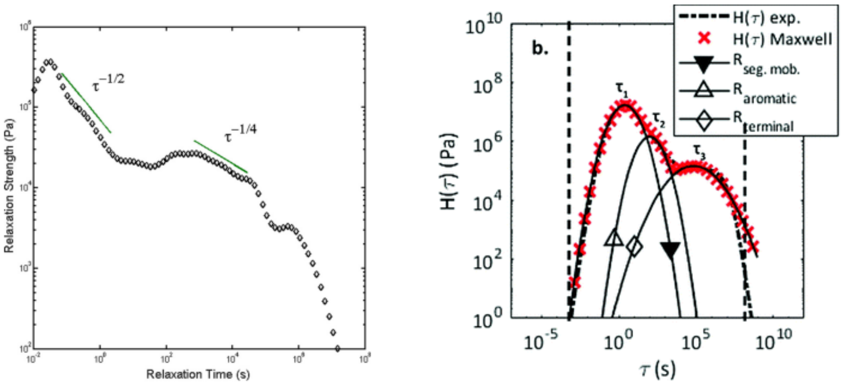

(a) (b)

Figure 2.3: Properties not directly distinguishable from other technique. (a) The two green lines show the characteristic power-law behaviors at short and long relaxation times. [18] (b) Contribution of different relaxation phenomena to the spectrum. [24]

Most recently, Montano et al. [24], utilized the spectra to understand the relaxation mechanism in a series of self-healing polyurethanes. Using a deconvolution model, were able to figure out how different, often overlapping relaxation phenomena contribute to the total relaxation energy curve. It was only possible by having a priori knowledge about the specific molecular structures Figure 2.3b.

2.1 THEORETICAL BACKGROUND

To obtain the Continuous relaxation spectrum, several steps are necessary.

First, the polymer master curve is needed: this curve shows the viscoelastic mechanical properties of the material (e.g., storage modulus, loss modulus, tan delta) with a broad range of frequency.

To acquire the experimental data, temperature-frequency sweep oscillation tests are required.

2.1.1 Master curve and TTS

The way to obtain a master curve is by executing oscillation tests in a dynamic mechanical analysis (DMA) machine. Three parameters are under control in this kind of test: frequency of oscillation, amplitude of oscillation, and test temperature. Generally, two of these parameters are held constant while the third is varied continuously. In this case, a temperature and a strain amplitude are selected, and then the frequency sweep test is run.

The test is repeated for different temperatures, an example of the results is shown in Figure 2.4.

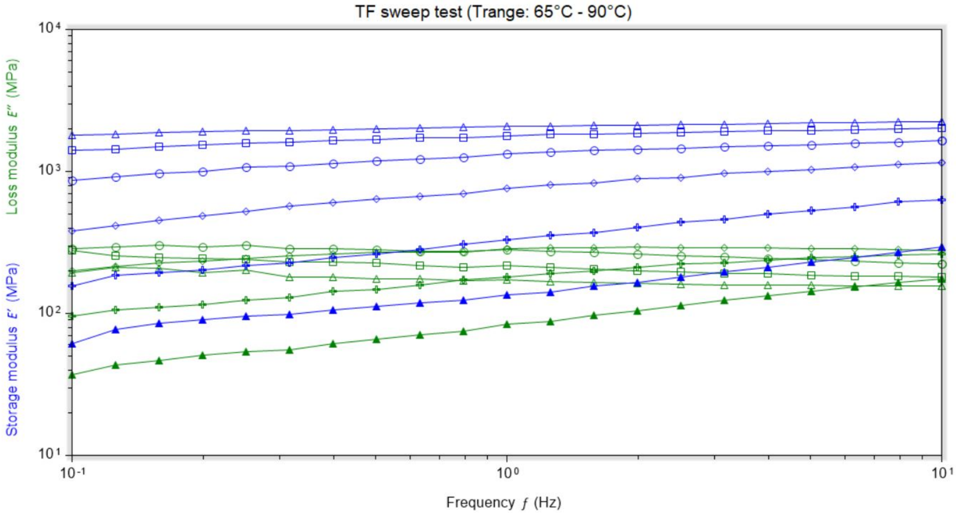

Figure 2.4: Temperature-frequency sweep test data: storage and loss moduli plotted against the frequency range, each line correspond to a different temperature step.

Using the time-temperature superposition (TTS) principle, once selected the model and the model reference temperature, is possible to shift horizontally every single curve obtained at a given temperature. Data collected at a temperature higher than the reference one will be shifted towards low frequencies and vice versa. In such a manner, the range of frequency covered by the mechanical data is wider than before Figure 2.5.

The core of the principle is based on the equivalence of time and temperature: long-time relaxation at a lower temperature is equivalent to short-time relaxation at a higher temperature. Thus, this method allows for predicting viscoelastic phenomena at a very long-time regime (and very short-time regime) by the measurements at various temperatures. Since every viscoelastic measuring device has a finite range of measurement, this principle permits to have a greater knowledge about the viscoelasticity of polymers [25].

The shifting model used in this work is the one proposed by Williams, Landel, and Ferry [26], it consists of an empirical relationship between the shift factor, a_T, and the temperature:

$$\ln a_T = -\frac{C_1(T - T_{ref})}{C_2 + (T - T_{ref})} \tag{2.1}$$

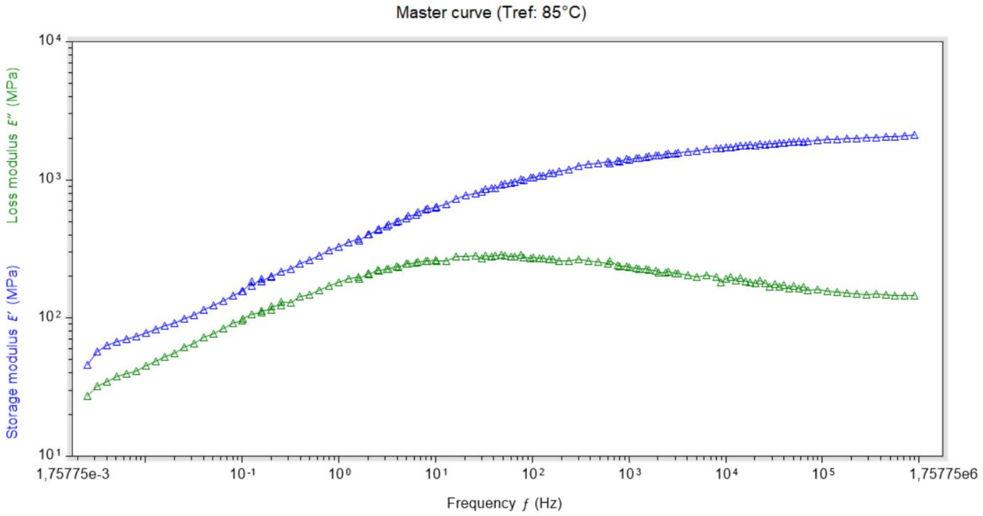

Figure 2.5: Master curve obtained from rheology data using the WLF model at a reference temperature of 85°C.

C_1 and C_2 are constants that depend on the material and on the reference temperature, T_{ref}. Theoretically, the TTS should not be performed near a transition temperature, since they depend on thermal history, but this model represents an exception. Originally the TTS principle has been developed for just thermorheologically simple materials, in which a change in mechanical properties due to a temperature change should be produced in the same way by a variation in frequency [27, 28]. Therefore, there is a limit on the material choice: TTS should be only appliable to homogeneous, isotropic, and amorphous samples and the material should remain within the linear viscoelastic range (LVR) under the deformation of interest. Despite this, it is being used increasingly to analyze the behavior of a more complex and branched system [29, 30] and in literature there are contrasting opinion about its correct use.

2.1.2 From the master curve to the CRS

The CRS is obtained from the rheological data of the storage and loss moduli through the inversion of the Fredholm equations:

$$G'(\omega) = \int_0^\infty H(\tau)\frac{\omega^2\tau^2}{1+\omega^2\tau^2}\frac{d\tau}{\tau} \tag{2.2}$$

$$G''(\omega) = \int_0^\infty H(\tau)\frac{\omega\tau}{1+\omega^2\tau^2}\frac{d\tau}{\tau} \tag{2.3}$$

Here, the shear storage modulus G' and the shear loss modulus G'' are expressed in function of the relaxation modulus, the angular frequency (ω) and the relaxation time.

The solution represents an ill-posed problem; many procedures have been proposed to overcome this issue [18], but due to its simplicity and online availability, the non-linear regression method of Honerkamp and Weese is one of the most used [23].

In their solution the logarithm of the spectrum is considered, since the short and the long relaxation time have considerably different contributions. A similar set of equations is obtained:

$$G'(\omega) = \int_{-\infty}^\infty \frac{\omega^2\tau^2}{1+\omega^2\tau^2}10^{h(\tau)}\frac{d\tau}{\tau} \tag{2.4}$$

$$G''(\omega) = \int_{-\infty}^{\infty} \frac{\omega\tau}{1+\omega^2\tau^2} 10^{h(\tau)} \frac{d\tau}{\tau} \tag{2.5}$$

An estimate for the logarithm of the spectrum $h(\tau) = \log H(\tau)$ is obtained employing the basic concept of the Tikhonov regularization, by minimizing:

$$\begin{aligned} V(\lambda) = \sum_{i=1}^{n} \frac{1}{\sigma_i'^2} \left[G_i'^{\sigma} - \left(\int_{-\infty}^{\infty} \frac{\omega_i^2\tau^2}{1+\omega_i^2\tau^2} 10^{h(\tau)} \frac{d\tau}{\tau} \right) \right]^2 + \\ + \sum_{i=1}^{n} \frac{1}{\sigma''^2_i} \left[G''^{\sigma}_i - \left(\int_{-\infty}^{\infty} \frac{\omega_i\tau}{1+\omega_i^2\tau^2} 10^{h(\tau)} \frac{d\tau}{\tau} \right) \right]^2 + \\ + \lambda \int_{-\infty}^{\infty} \left(\frac{d^2}{d\tau^2} h(\tau) \right)^2 \frac{d\tau}{\tau} \end{aligned} \tag{2.6}$$

where $G_1'^{\sigma}$,...,$G_n'^{\sigma}$, G''^{σ}_1,...,G''^{σ}_n denote the experimental data for $G'(\omega_1)$,...,$G'(\omega_n)$, $G''(\omega_1)$,...,$G''(\omega_n)$ and σ_1',...,σ_n',σ''_1,...,σ''_n are the corresponding errors.

The results from the first and second terms on the right side are forced to be compatible with the experimental data, after the choice of an appropriate regularization parameter λ.

The TTS master curve and the conversion into the continuous relaxation spectra, in this work, are achieved using TA instruments TRIOS software installed in the TA instruments DMA machine. Since a tensile geometry is used to perform the oscillation tests, the software executes an ulterior step: the shear storage and loss moduli G', G'' are substituted with the storage and loss modulus E' and E'' applying the well-known relationship between G and E [31].

3 EXPERIMENTAL SECTION

3.1 MATERIALS

Bisphenol A diglycidyl ether (DGEBA) in the form of Epikote 828 resin (184-190g eq-1) and Ancamine 2500 curing agent (105-110 g eq-1) were provided by Akzo Nobel Aerospace Coatings and used as received. Since the Ancamine 2500 is a commercial product, not all the amine monomer constituents are known except for the aminoethylpiperazine. The correspondent chemical structures are reported in Figure 3.1.

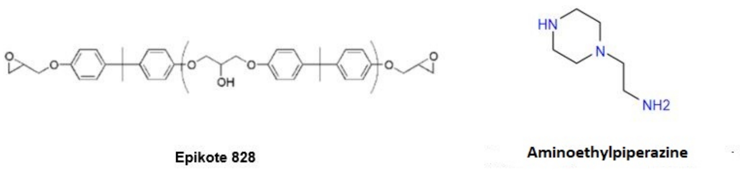

Figure 3.1: Chemical structures of Epikote 828 and aminoethylpiperazine (the only monomer known in the Ancamine 2500).

The epoxy-amine system chosen is a common base composition for aircraft coatings, hence a great knowledge of the synthesis procedure and its characteristics is available. In addition, this system was already used as a reference polymer in Roth's research, making possible a comparison of the results.

To form the thermosetting polymer network, the amine group of the hardener will react with the epoxy group of the resin in multiple additions, as shown in Figure 3.2:

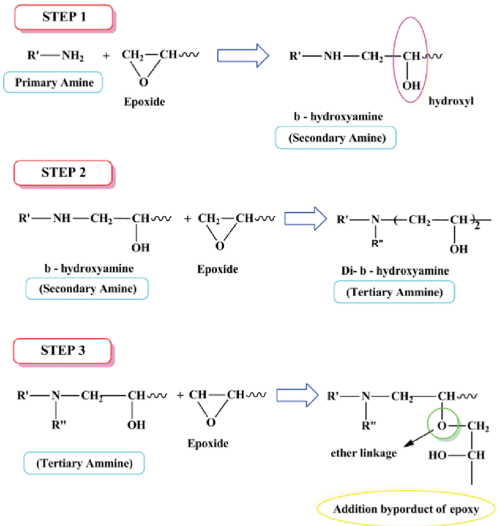

Figure 3.2: Addition reaction mechanism of a generic DGEBA epoxy resin mixed with an amine hardener. [32]

1. First, the amine will react with the epoxide group, bringing to the opening of the epoxy ring and to the formation of the secondary amine;

2. The secondary amine will react, ideally, with another epoxide group, forming the epoxy junction point;

3. Another unwanted addition product can be formed with the reaction of the hydroxyl group with the epoxide.

The Epikote and the Ancamine have been mixed at the stoichiometric ratio (1 - 0.70).

3.1.1 Polymer synthesis and specimens preparation

The first step consists in weighting the necessary amounts of resin and hardener in two different jar and lowering their viscosity, putting them in the oven at 80°C (the resin for 15 minutes and the ancamine for the last two, as seen elsewhere [33]). The hardener is then added to the Epikote. After approximately 1 minute of mixing by hand, the mixture is put in the vacuum high-speed mixer for 4 minutes. The first minute is used to degas the jar and let the pressure inside the chamber decrease. Then, the mixture is stirred for 3 minutes at 800rpm. Finally, the mixture is poured into a Teflon mold and spread using a common steel rod. The length, width, and thickness of the mold's cavity are respectively (220 x 220 x 0.2) mm and at the end of the process thin samples will be obtained. The mold also, is tightened to a 5 mm aluminum plate to ensure a high level of flatness. The unevenness of the surface where the mold was put on, was checked by using a water level and adjusted using paper pieces.

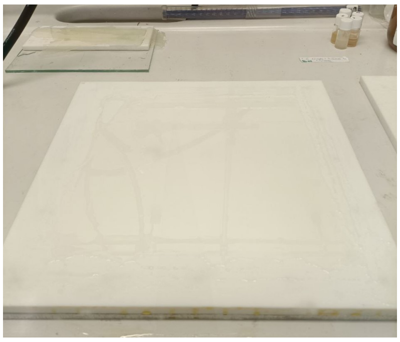

Figure 3.3: Teflon mold of (220 x 220 x 0.2) mm.

The mixture is allowed to cure at room temperature in the fume hood (20°C) for 24h. A thin film is obtained, to make the material softer and easier to cut, it is put in the oven at 100°C for 5 minutes. After removing the film from the mold, dog-bone samples are obtained using the Gibitre Die-cutting machine supported with an ASTM D1708 standard cutter.

Cutting them before the second curing step, allow to remove residual stresses induced by the cutting, since a sort of thermal treatment, above the material Tg, is executed with the post-cure.

The samples are so placed on a Teflon tray and put in the oven at 100°C for 24h to complete the curing process, after that they are allowed to cool down at room temperature in the fume hood.

When the cooling is completed, the dog bones are stored, in a cup without the lid, inside a desiccator containing silica gel grains, to avoid humidity effects.

Two different batches (A and B) have been realized following the same procedure.

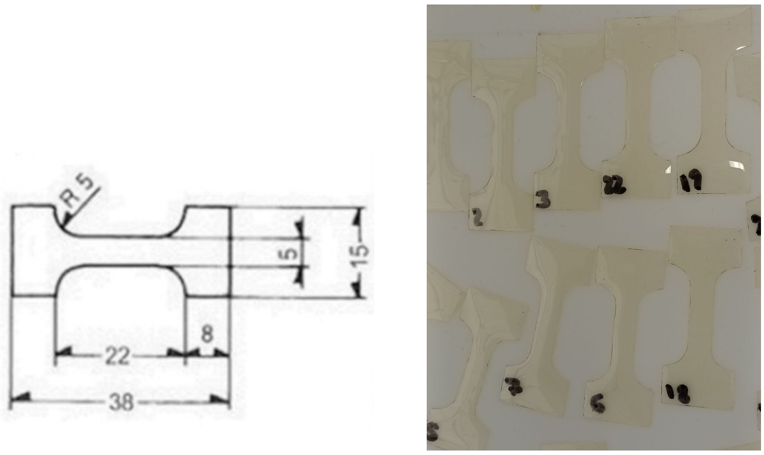

(a)

(b)

Figure 3.4: (a) Samples dimensions; (b) Dog-bone shaped samples after cutting.

3.2 CHARACTERIZATION METHOD

3.2.1 Thermal gravimetric analysis (TGA)

Temperature sweep tests are conducted on a Perkin Elmer TGA 4000, from 20°C to 500°C, to verify the thermal stability of the polymer. The heating rate used is 10°C/min. The tests are executed in a Nitrogen controlled environment. The temperature at the 1% weight loss (1wt%) point is taken as the maximum limit for the execution of the subsequent experiments, in order to get reliable results.

3.2.2 Differential scanning calorimetry (DSC)

Temperature ramp tests are executed on a TA instrument DSC250 machine to measure thermal transition temperatures. The tests started from 0°C and reached 140°C. Two heating ramps under Nitrogen are run with a 10°C/min rate, separated by a cooling ramp with a 5°C/min rate. The glass transition temperature (Tg) is taken from the second heating ramp curve since the first one is used to remove the thermal history of the specimen. The Tg is selected as the midpoint of the endothermic event.

The DSC is also used to verify the effects of the temperature-frequency sweep test and oven treatment test on the samples Tg.

3.2.3 Dynamic mechanical analysis (DMA): temperature sweep

A temperature sweep is executed on a TA instrument RSA-G2 DMA machine. Data of the storage and loss moduli and delta function are collected from 20°C to 140°C at a heating rate of 2°C/min, a frequency of 10Hz, and a strain of 0.1%. The temperature at the peak of the tan delta will be used as a reference in WLF model.

3.2.4 Tensile test

The samples were tested at room temperature, at a constant crosshead speed of 0.5mm/min, using an Instron 3365 tensile test machine implemented with a 1kN load cell. The same machine is used to damage the samples inducing a plastic strain.

3.2.5 From DMA TF sweeps test to CRS

The spectra are obtained following three steps:

1. Execution of the TF sweep test on the DMA;
2. Construction of the TTS master curve;
3. Conversion into the CRS.

TF sweep test

Temperature-frequency sweep tests are performed, to set the protocol, at different starting temperatures (Ts):

- 20°C, room temperature;
- 65°C, beginning of the transition zone;
- 45°C, a temperature in between.

The temperatures are selected by looking at the preliminary temperature ramp test: the range of interest is the one that includes the main relaxation phenomenon where the major effects of damage are expected to be seen since more energy is dissipated in this area.

The range of the temperature used is Ts-100°C with a 5°C/step. At each temperature, a frequency sweep is executed from 0.1Hz to 10Hz in 10 logarithmic steps per decade and the sample is loaded at 0.1% of strain (strain previously checked with an amplitude sweep test to confirm the linear viscoelastic range).

Samples are clamped in a tension geometry setup with a 10 mm loading gap, as depicted in Figure 3.5. The tightening torque of each bolt is checked with a torque wrench (30 cNm). The tests are performed in a climate chamber under Nitrogen.

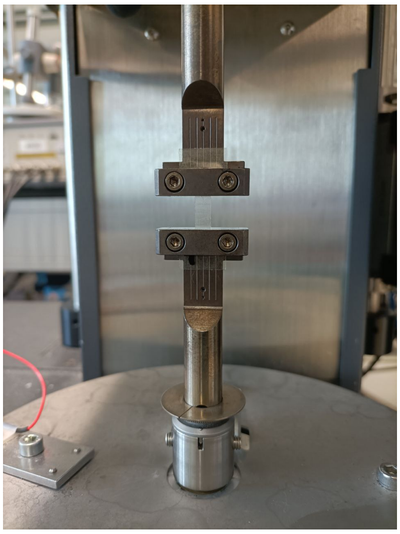

Figure 3.5: Set-up of the RSA-G2 DMA machine with the tensile geometry.

TTS master curve

Data from the rheological tests are used in TA Instruments TRIOS software, to apply the time-temperature superposition principle: storage and loss modulus data are frequency shifted using a WLF shifting model and 85°C as a reference temperature. This temperature corresponds to the loss modulus peak on the DMA temperature sweep. To confirm the validity of the master curves, the horizontal shift factor curve trend is observed: it must be a descending line when plotted logarithmically with the temperature. The software can also execute the linear regression of the curve and by looking at the fit factor (shifting fit factor) obtained, is possible to see how far experimental data are from the ideal shifting conditions. The test starting temperature will be selected by looking at the best shifting fit factor obtained in the preliminary experiments.

CRS

It is possible to generate the spectra automatically from the master curves by exploiting the functionality of the TRIOS software. Using the continuous stress relaxation analysis, TRIOS will first, approximate the rheology data with the nearest curve, providing a fit factor (CRS fit factor), and then apply the model described in Chapter 2.

Relaxation time at the peak, peak height, and area under the complete spectra are taken as curves comparison parameters (Fig. 3.6).

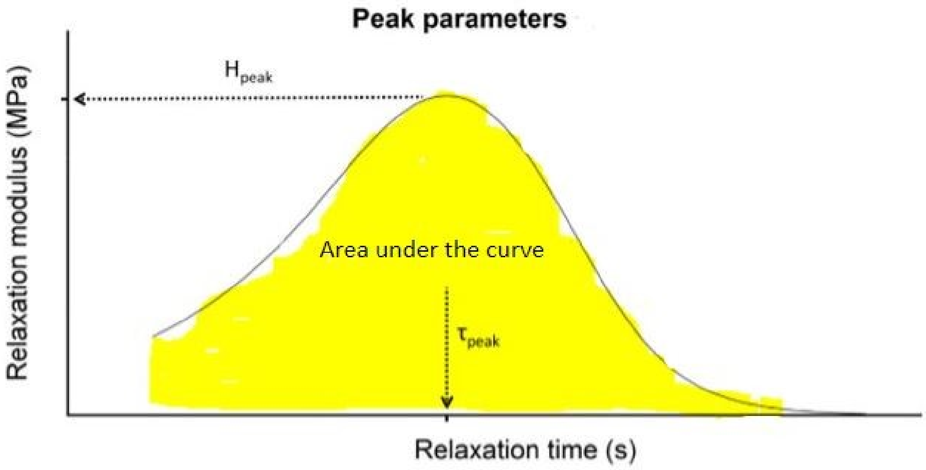

Figure 3.6: Description of peak parameters.

3.3 PROCEDURE

3.3.1 Pristine state

Six pristine samples from two different batches have been tested using the DMA protocol previously described. They represent the baseline to compare all the experiments.

Sample	Step 1	Step 2
A1,A2,A3	TF sweep	CRS protocol
B1,B2,B3	TF sweep	CRS protocol

3.3.2 Damaged state

Six samples taken from the two different batches are first damaged, inducing a strain of ca. 2%, through the use of the Instron 3365 machine. Three of them are tested with the DMA 10 minutes after the damaging step (approximately the necessary amount of time required to set up the DMA machine for the TF sweep test), the others, after 1 week of recovery time. The recovery time in between can be seen as an 'healing period' at room temperature.

To select the straining value, first, was necessary to look at the sigma-epsilon curves obtained with the tensile tests: once determined the highest value of strain at the yield point (approximately 1%) and the lowest value of strain at the breaking point (2.2%), it was possible to select the level of deformation within this interval, as much possible closet to the failure point, to be sure of straining the samples out of their elastic region.

Sample	Step 1	Recovery time	Step 2	Step 3
A1-m,B1-m,B2-m	Straining	10 minutes	TF sweep	CRS protocol
A1-w,A2-w,B1-w,B2-w	Straining	1 week	TF sweep	CRS protocol

3.3.3 Oven treatment

An oven treatment of 1 hour at the temperature of 85°C is executed on both pristine and damaged samples positioned on a Teflon tray. After that, three different cooling mechanisms are experimented with:

- Slow cooling: the sample remains in the oven with its door half-open, after 1 hour it is allowed to acclimatize at room temperature;
- Soft quench: the sample is allowed to acclimatize directly at room temperature after the treatment;
- Quench: the sample is put in a fridge at 4°C for 10 minutes, and then is allowed to reach room temperature. It has been stored in a closed plastic bag to minimize the humidity effects of the low temperature.

During the cooling, the temperature is monitored with an RS-PRO K type thermometer equipped with thermocouples. The electrical conductors are fixed on the sample using a common Teflon tape (Fig. 3.7).
The TF sweep test is then executed, in all the cases, after 48 hours from the oven treatment.

Sample	Step 1	Step 2	Cooling	Rec.time	Step 3	Step 4
B-s	x	1h 85°C	Slow	48h	TF sweep	CRS
B-Ds	Straining	1h 85°C	Slow	48h	TF sweep	CRS
B-sq	x	1h 85°C	Soft quench	48h	TF sweep	CRS
B-Dsq	Straining	1h 85°C	Soft quench	48h	TF sweep	CRS
B-q	x	1h 85°C	Quench	48h	TF sweep	CRS
B-Dq	Straining	1h 85°C	Quench	48h	TF sweep	CRS

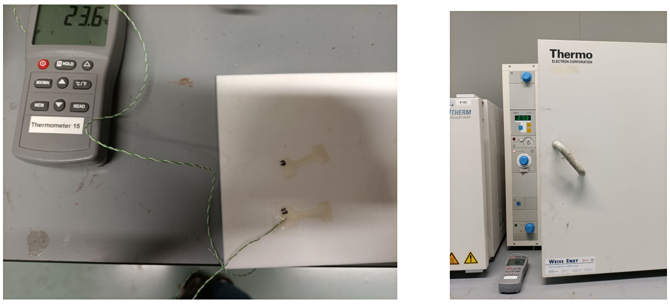

(a) (b)

Figure 3.7: (a) Thermocouples setting; (b) Slow cooling with the oven door opened.

4 RESULTS

4.1 THERMAL CHARACTERIZATION

Five TGA tests in total were executed, two from the first batch (A) and three from the second (B). The samples have been taken from different areas of the polymers to value the homogeneity; their starting weight is within 4-8mg.

In Figure 4.1 a range of almost 10°C is identified and the 1wt% weight loss is taken as the average value, the error bar indicates the scatter between the tests based on the standard deviation.

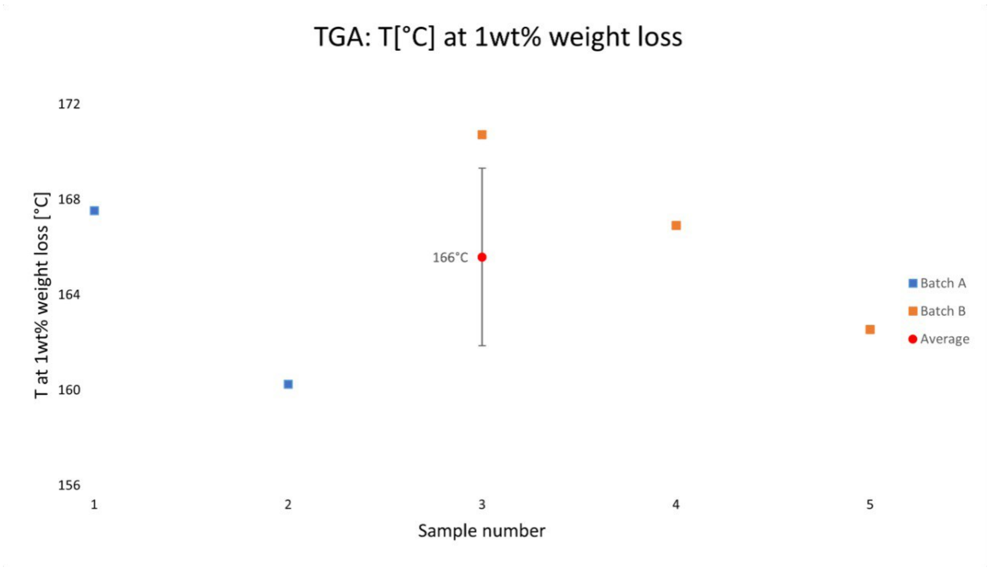

Figure 4.1: Temperature at the 1wt% weight loss reached by each samples during the TGA test.

The high temperatures reached at the beginning of degradation, suggest that no by-products like water are present in the polymer. Hence, the results reveal that the developed films are thermally stable at the temperature chosen for the TF sweep tests. The graphs obtained from each test can be found in the Appendix.

The thermogravimetric analysis also, permits the selection of a reasonable maximum temperature for the DSC test, in this case, set at 140°C.
DSC is used to determine the polymer's glass-transition temperature and to assess the goodness of the curing process.

A single endothermic event related to glass transition is registered: the Tg is taken from the second heating ramp as the half-height of the transition range (Fig.4.3). The values are reported in the following table for each sample, considering the Tg associated with the first heating ramp as well.

Sample	**Tg 1st heating ramp [°C]**	**Tg 2nd heating ramp [°C]**
DSC-A1	72	75
DSC-B1	69	74
DSC-B2	71	77
DSC-B3	71	75

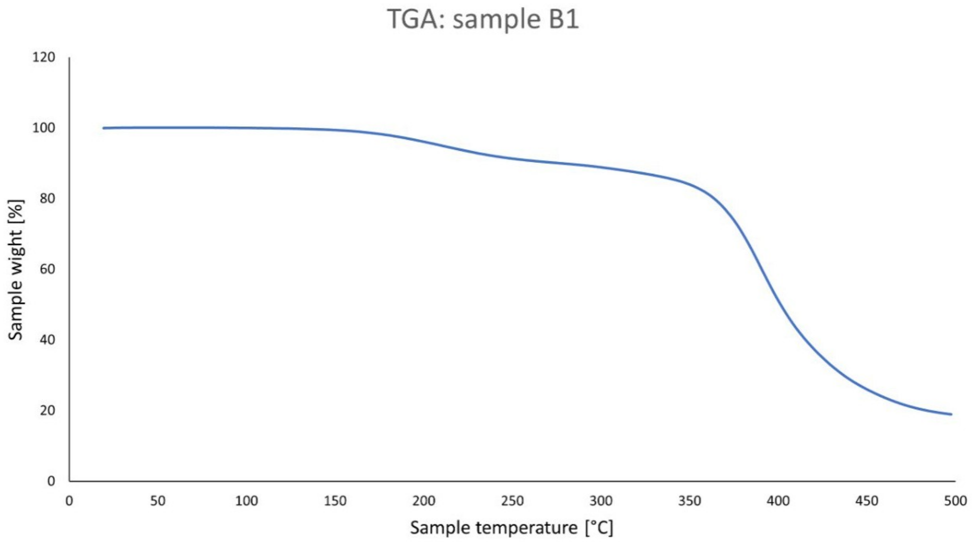

Figure 4.2: Sample weight (TGA-B1) in percentage during the TGA temperature ramp.

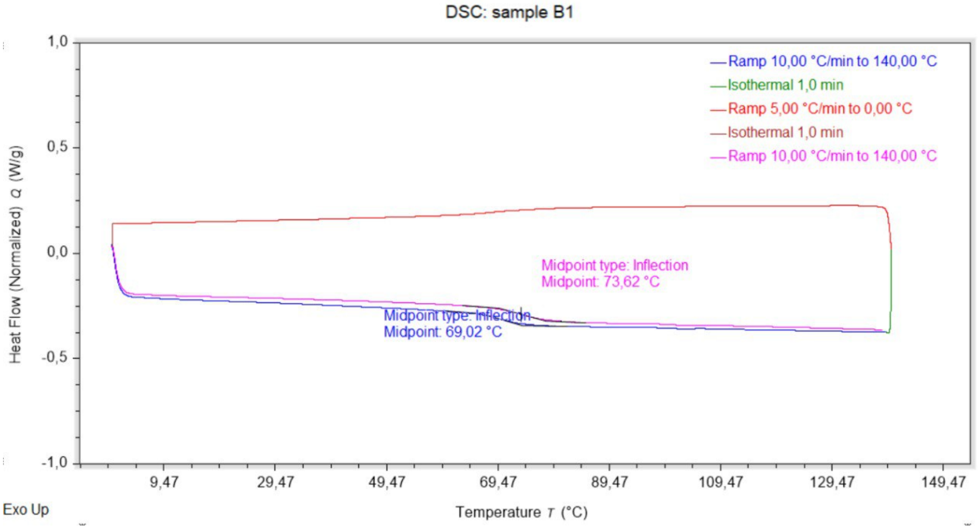

Figure 4.3: Sample (DSC-B1) heat flow during the DSC test.

Comparing the two heating ramps (example in figure 4.3), changes in the Tg are evident. They are due to the polymer's post-curing effects: when heating to a higher temperature during the first scan (140°C), the frozen state relaxes, and the polymer can reach its true Tg [34].

An average Tg value among the four tests executed, which corresponds to 75°C, is calculated.

The scatter in the data can be attributed to the mixture of amines that are used to form the network, leading to more network heterogeneity and local variation in crosslinking density [33].

DMA temperature sweep results are shown in fig. 4.4. The unique transition is also apparent when examining the temperature dependence of the dynamic moduli. The temperature at the loss modulus peak, is taken as WLF reference [24, 15], (85°C).

Moduli behavior with time is consistent with a highly crosslinked thermoset [35]: the transition zone separates glassy and rubbery regimes characterized by a decreasing of the E′ values, from ca. 2,5GPa to several MPa.

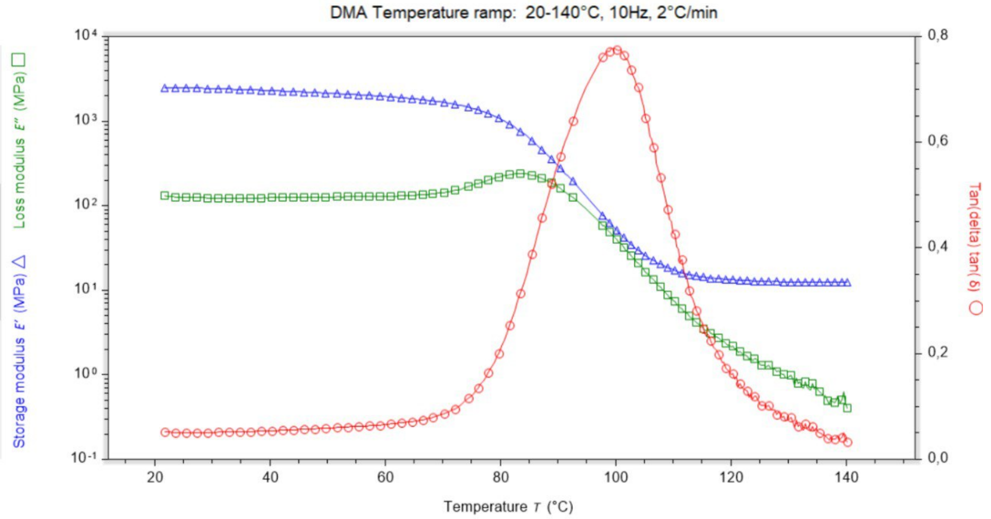

Figure 4.4: DMA temperature run executed from 20°C to 140°C, with a temperature step of 2°C/min at a frequency of 10Hz.

4.2 TENSILE TEST

Three dog bones specimens from batch A have been tested fig. 4.5. The values of the corresponding E modulus, strain at yield point, and point of break are reported in the table below.

Another indication of the network heterogeneity could be shown by looking at the different strain at failure reached by the samples, but also, a not accurate alignment of the specimen, or the difference in the not hydraulically controlled pressure impressed by the clamps, could have affected the results.

Sample	Young Modulus [MPa]	Strain at break[%]	Yield point[%]
1	4662	2.42	1
2	4580	2.18	0.9
3	4559	2.95	0.8

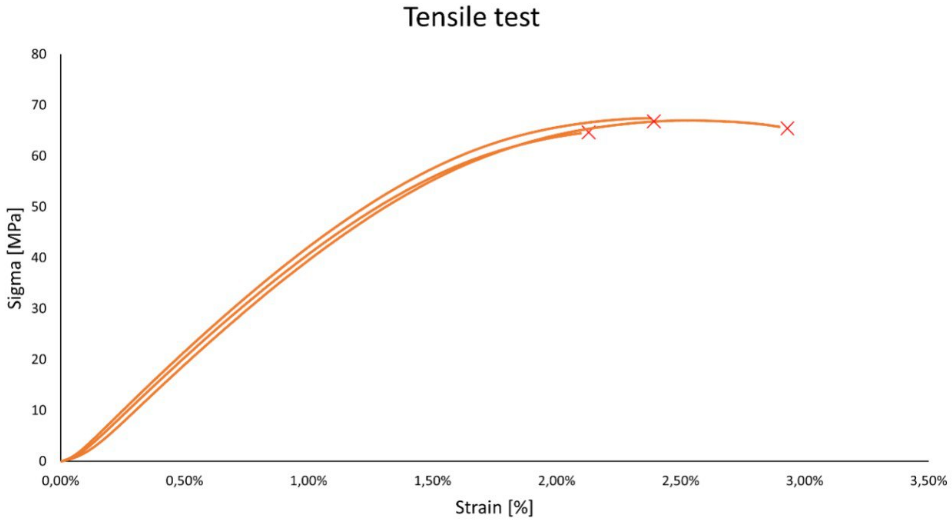

Figure 4.5: Stress-strain of 3 dog-bone samples from batch A.

After establishing the highest value of strain at the yield point (ca. 1.00%) and the lowest value of strain at the breaking point (2.18%), the strain level to use to damage the samples is selected (2%). This value of strain allows inducing permanent damage in the network without reaching the breaking point. The elastic modulus was determined by fitting the initial linear region (between elongation 0.2% and 0.5%) of the stress-strain curve.

4.3 DMA PROTOCOL

4.3.1 Test starting temperature

The first experiments conducted with the DMA were helpful in defining the most suitable protocol to use when testing the samples. One of the first parameters that were evaluated was the temperature range used when performing the TF sweep test.

Comparing the fit factors obtained in three tests with three different starting temperatures some considerations were made (figure 4.6).

It was noted that if the starting temperature used is close to the transition zone (45°C, 65°C), the data obtained have lower reliability that can be quantified, as explained above, by the shifting fit factor obtained while performing the linear regression of the aT parameter curve. Starting the tests from a lower temperature shows improvements in the fitting parameter.

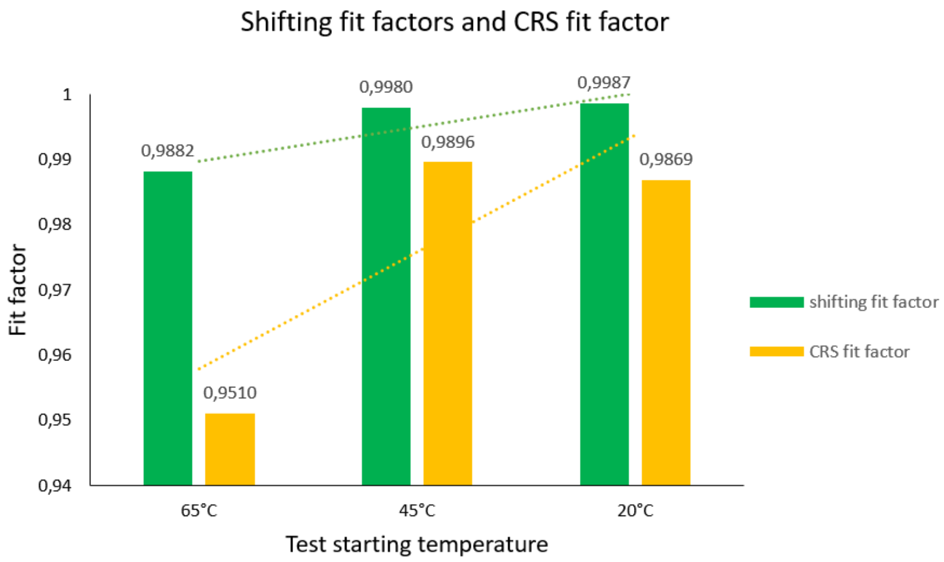

Figure 4.6: Shifting fit factor and CRS fit factor obtained for tests with a different starting temperature.

The greatest degree of improvement is achieved by moving from 65°C to 45°C, the former is at the beginning of the transition zone. The test that showed the best results was the one conducted at 20°C, which corresponds to room temperature.

This behavior is due not to the larger temperature range used, but rather to the chosen starting temperature. By setting a higher starting temperature, the chamber will reach that temperature in a relatively short time, in the order of tens of seconds. The sudden heating of the sample does not allow the network to adapt to the temperature gradually, and the first measurements will be taken when it has not yet reached the internal equilibrium. In addition, the machine's control system is also forced to respond more quickly in order to adapt to the new axial tension required and not allow the specimen to buckle.

Sample buckling is probably the most influential problem on the quality of the results.

The goodness of the CRS fit factor considerably increases as well, when starting the test from 45°C and it slightly decreases when the test begins at room temperature.

Finally, the temperature selected to conduct the subsequent tests is 20°C, this way allows also to avoid the sample's preconditioning in the climate chamber.

4.3.2 Shifting temperature range

The shifting range does not correspond to the testing range for different reasons.

First of all, the data acquired at a lower temperature tends to be overlapped or noisy, since the storage modulus is not significantly changing with the temperature and the loss modulus curves have the same tendency since the viscous behavior is not yet predominant.

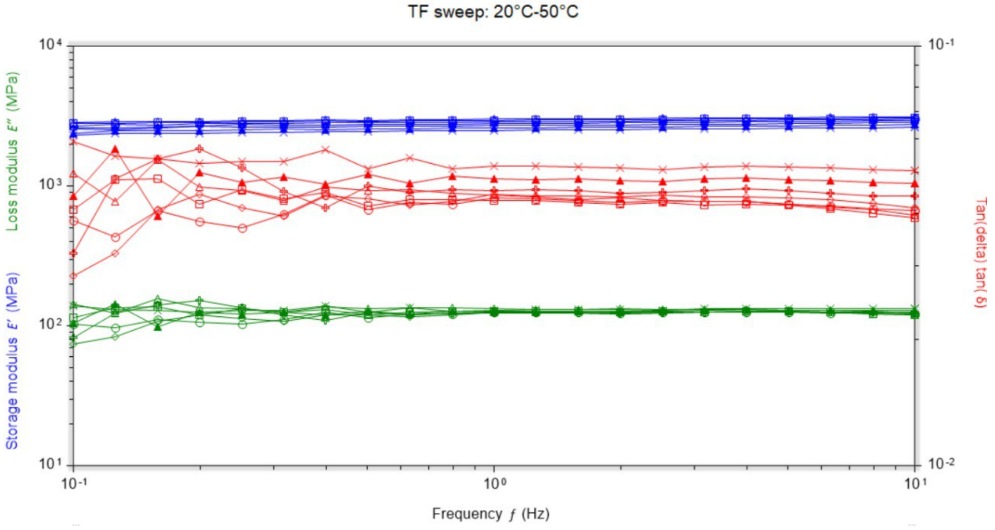

Figure 4.7: Storage modulus, loss modulus and loss factor data from a TF sweep collected in the low-temperature range.

The noise in the data will turn into frequency bumpiness in the master curve, as shown in the figure below 4.8.

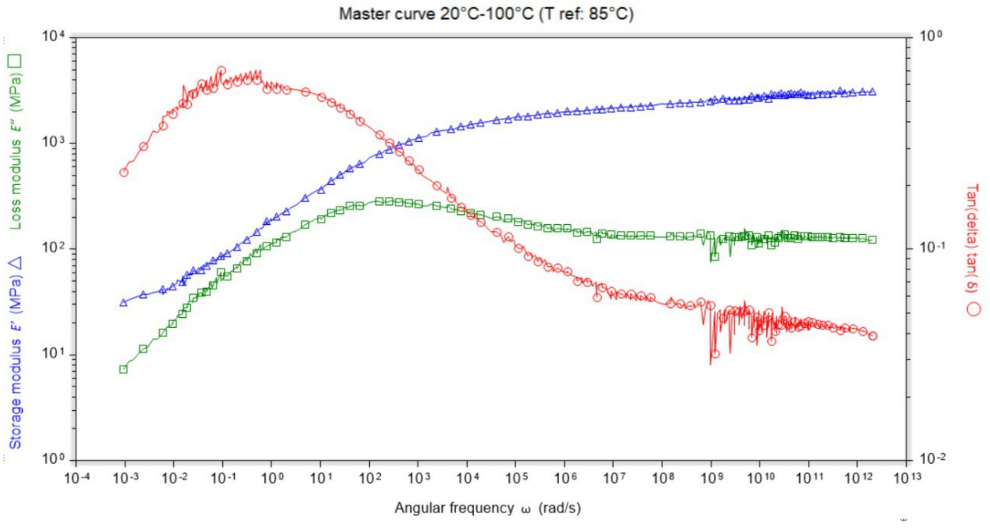

Figure 4.8: High-frequency bumpiness found in the master curve, obtained from the frequency sweep at low temperatures.

While the global curve approximation can obtain a good fit factor, locally it may depends. The bumpiness found in the master curve will appear in the relaxation spectrum as well at the correspondent times (fig. 4.9).

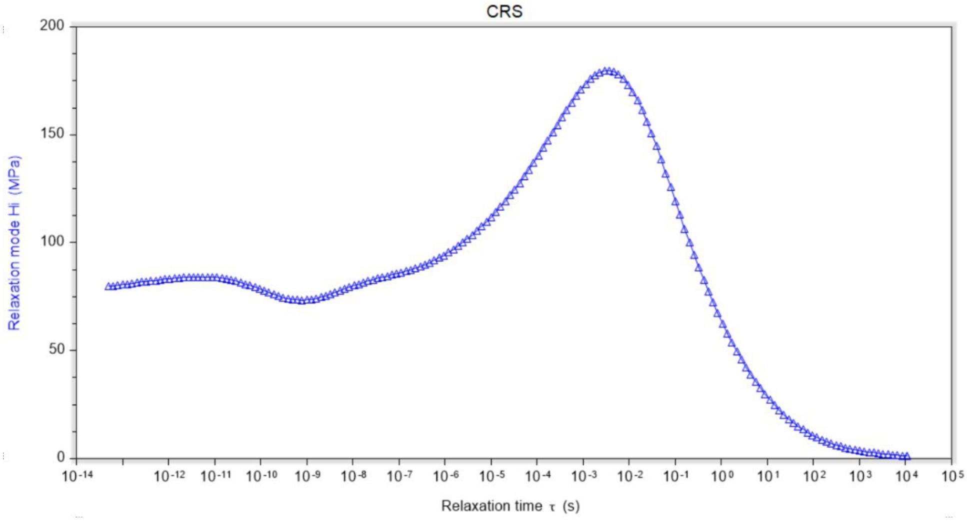

Figure 4.9: Master curve obtained applying WLF shifting model at a reference temperature of 85°C in the range 20°-100°C.

In addition, looking at the aT shifting factor curve (fig. 4.21), it is characterized by irregular changes in slope. In those temperature ranges, therefore, the data and the shifting cannot be considered reliable (even more so since the WLF model is designed for temperature between Tg and Tg + 100°C).

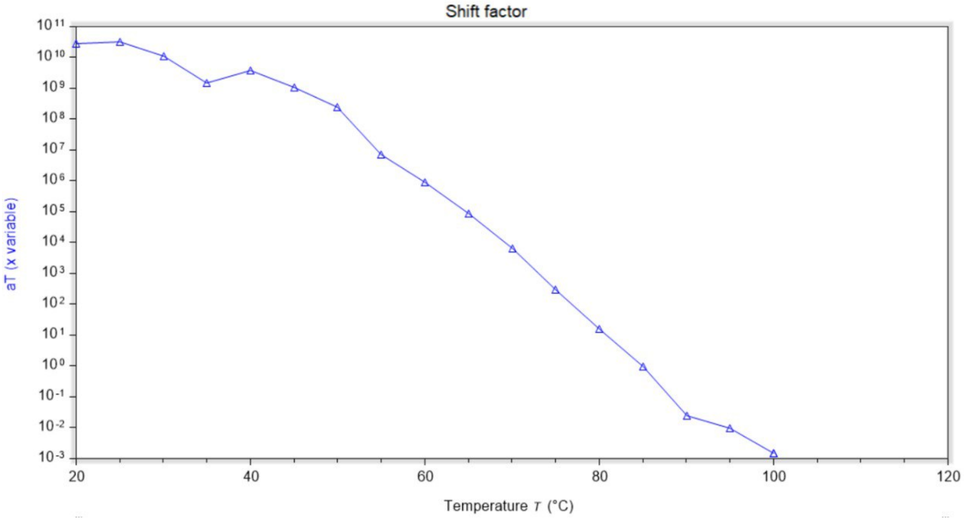

Figure 4.10: aT shift factor curve shifting data collected between 20°C and 100°C.

However, from the plot, it is possible to distinguish a region in which the behavior of the curve is ideal: 65°C-90°C. This is the shift range that will be used for the construction of the master curves of all subsequent tests. The relaxation peak of interest falls within this range. It should be noted again that the temperature ramp to which the test specimens will be subjected is instead 20°C-100°C.

Reducing the range of frequencies over which the master curve will be constructed will also result in a better local approximation of the data.

4.4 PRISTINE STATE

The figures below (fig. 4.11,4.12) show the stress relaxation spectra obtained from the pristine state samples after the TF sweep test. Three specimens for each batch have been tested (not necessarily on the same days).

Looking at the peak parameters obtained separately from the two batches, it can be seen that, in both cases, each specimen tested is an outlier of a different type (relaxation time, height, or area) and it is not possible to discard any of them. However, the range of the results obtained from the two families of samples is comparable as well as the deviation associated with the average values (fig.4.13).

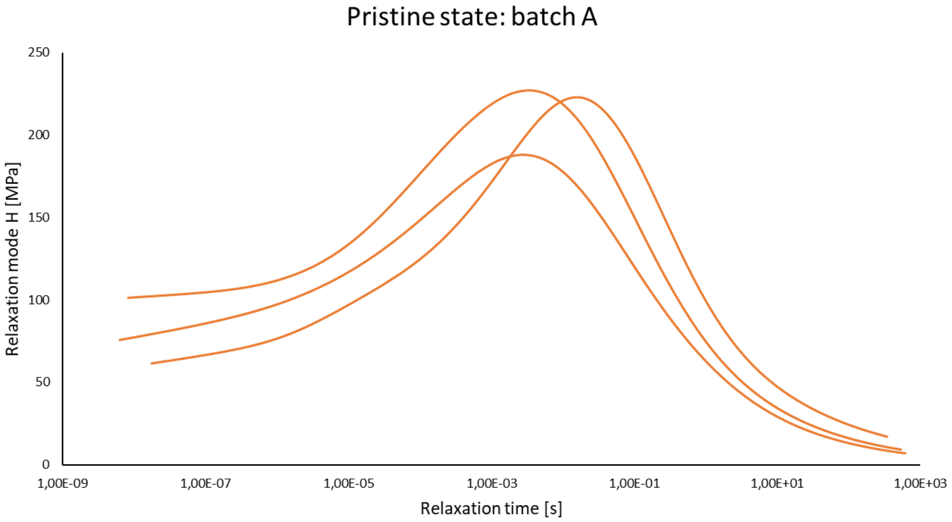

Figure 4.11: CRS obtained for pristine state samples (batch A).

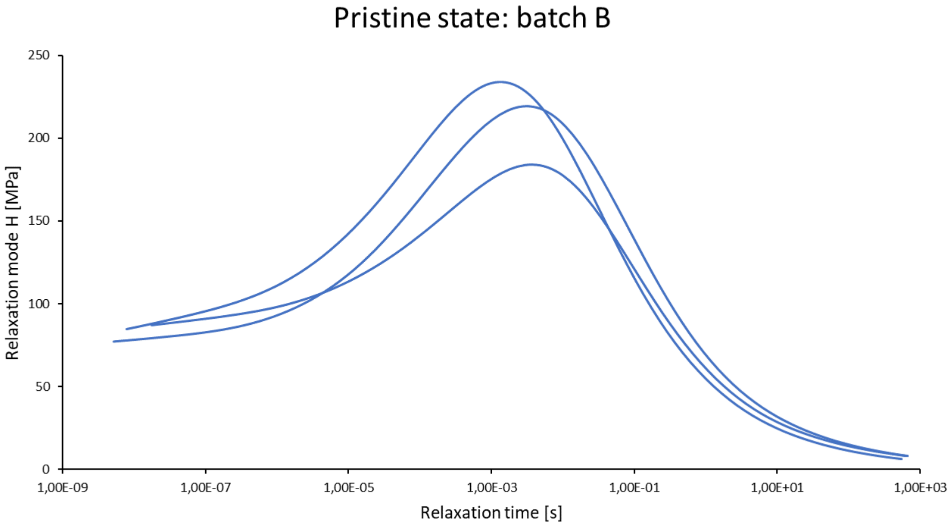

Figure 4.12: CRS obtained for pristine state samples (batch B).

The main difference between the two batches turns out to be the relaxation time: batch A shows slightly higher relaxation times.

For the six samples, the peak height varies from 186 to 227 MPa, the average relaxation time at the peak is in the order of 10^{-3} , and the average subtended area is 1167 MPaLog(s).

One question that arises is what the variability of the curves is due to.

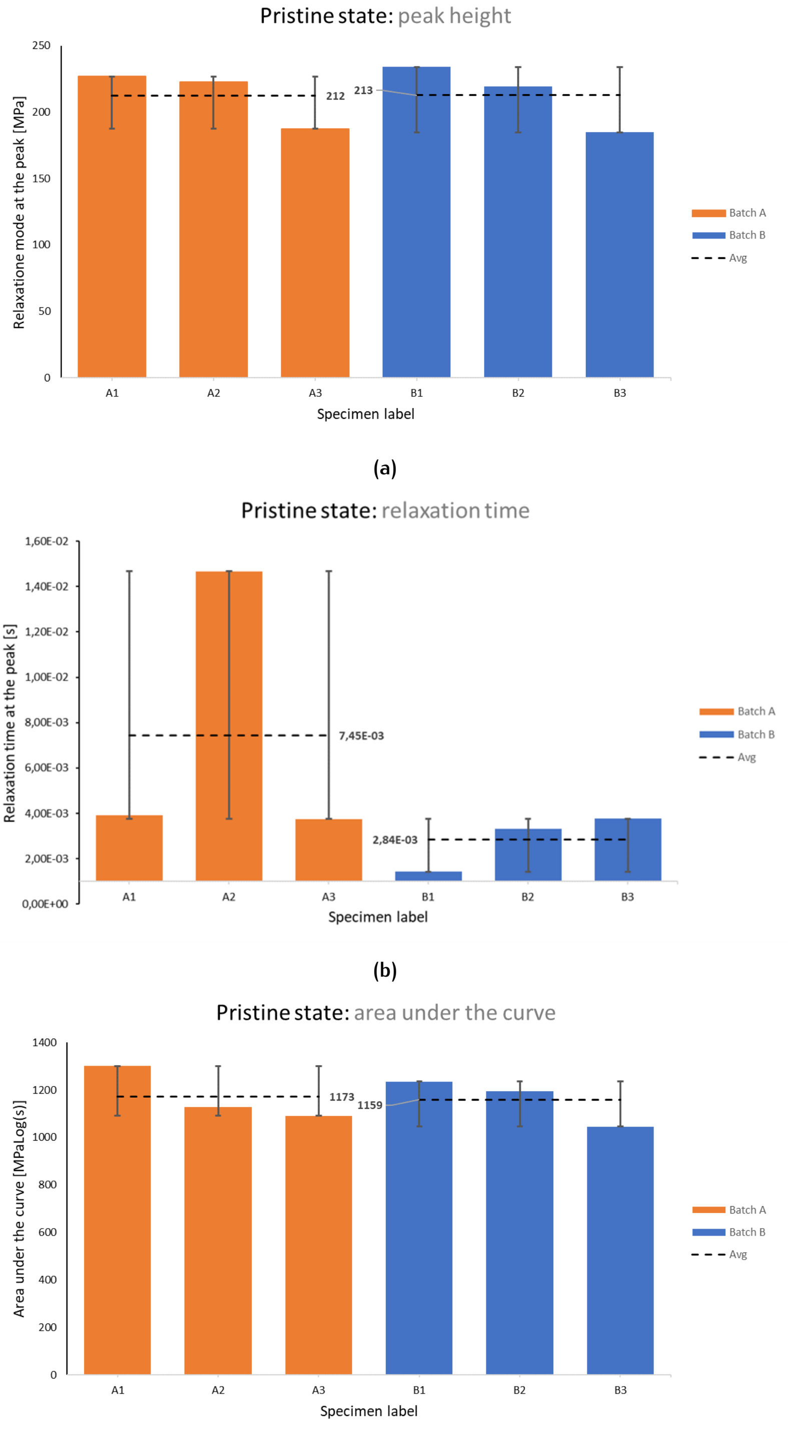

(a)

(b)

(c)

Figure 4.13: Pristine state peak parameters: the error bars are associated to the maximum value and minimum value of the considered parameter, the dashed lines represent the mean value. (a) Relaxation mode at the height. (b) Relaxation time at the peak. (c) Total relaxation energy.

The samples underwent the same thermal history and were subjected to the same storage conditions. The cutting step could affect the internal stress state, but by performing the second step of curing, the effects of cutting should have been removed. The specimens from batch B in particular were selected so that they belonged to the same mold area, for this reason the heat flux received should also be homogeneous. Specimen cross-section and thickness were found to have no correlation with the results obtained, as well as the date of the test (the samples from batch B have been tested on the same day).

A likely hypothesis remains the ability of the test to detect the inherent heterogeneity in amorphous polymers.

4.5 DAMAGED STATE

4.5.1 10 minutes recovery time

The specimens tested 10 minutes after damage show consistent results: the difference between the peaks is in the order of 1 MPa, and the distance from the mean value of the subtended area is at most 2.2%. More variations are found in the time factor: the specimen from batch A shows slightly longer relaxation times, the same trend was found in the pristine state specimens (fig. 4.14).

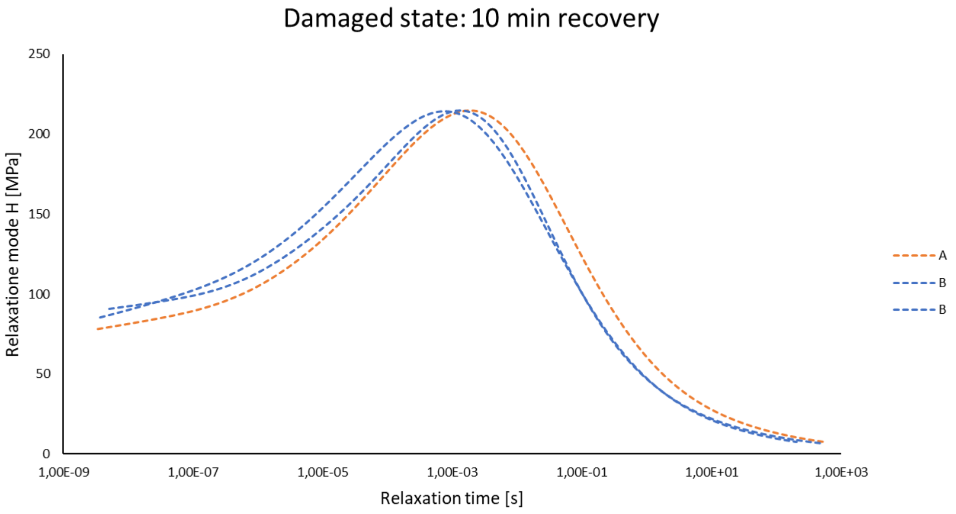

Figure 4.14: CRS obtained from samples tested 10 minutes after the damage.

The comparison between the pristine and damaged state peak parameters shows that the average value of the peak height is about the same and the area under the curve is slightly higher in the damaged specimens but in any case, the average values fall within the range of uncertainty associated with the measurements of the pristine state. The only exception is represented by the relaxation time, shorter in the damaged specimens (fig. 4.15) .

One would have expected, as a result of damage, a reduction in peak height or area under the curve, since having fewer bonds available and more dangling chains (elastically ineffective) decreases the storable energy in the specimens. Also, having fewer relaxation incentives, the stress response would have been expected to be shifted to longer relaxation times.

Probably the internal stress state induced by tensile testing is more responsible for the internal energy stored in the specimens than the number of bonds. During deformation, the internal equilibrium of the specimens is altered by trapping the

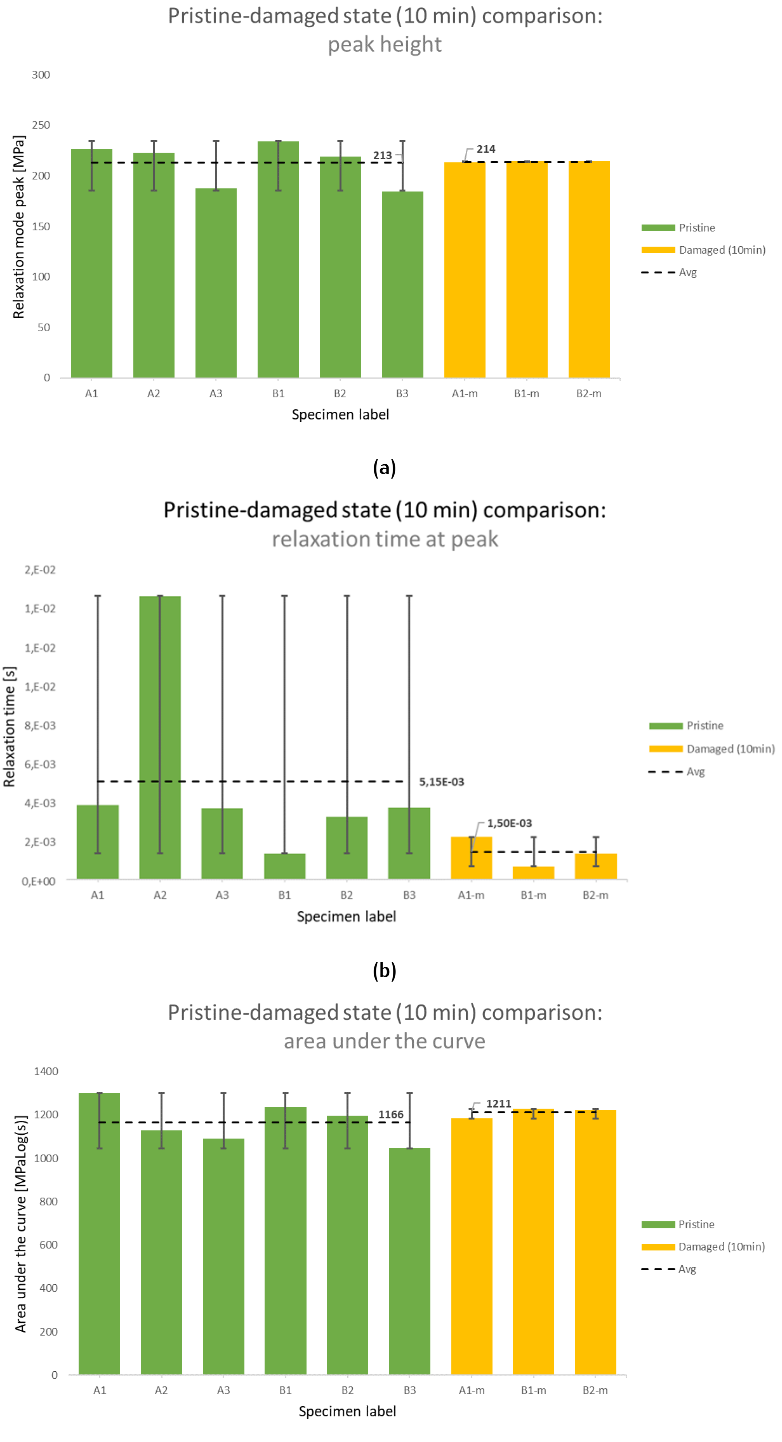

(a)

(b)

(c)

Figure 4.15: Damaged state (10 minutes) - Pristine state peak parameters: the error bars are associated to the maximum value and minimum value of the considered parameter, the dashed lines represent the mean value. (a) Relaxation mode at the height. (b) Relaxation time at the peak. (c) Total relaxation energy.

specimen in an unstable equilibrium position, and maybe, to get rid sooner of this unstable condition they tend to relax faster.

In addition, the deviation calculated for peak parameters in damaged samples is smaller than that of pristine samples. It seems that induced damage decreases the degree of heterogeneity found previously in the pristine state tests.

During the tensile test, the polymer chains will orient themselves in the direction of the load, acquiring a more organised position. Thus, the different orientation of the chains in the pristine sample, can be considered as a catchable factor of heterogeneity in the conducted tests.

4.5.2 1 week recovery time

More contrasting results are found in the data obtained for specimens tested after 1 week of recovery time, where in fact batches A and B show two different behaviors as shown in CRS plots (fig.4.16) .

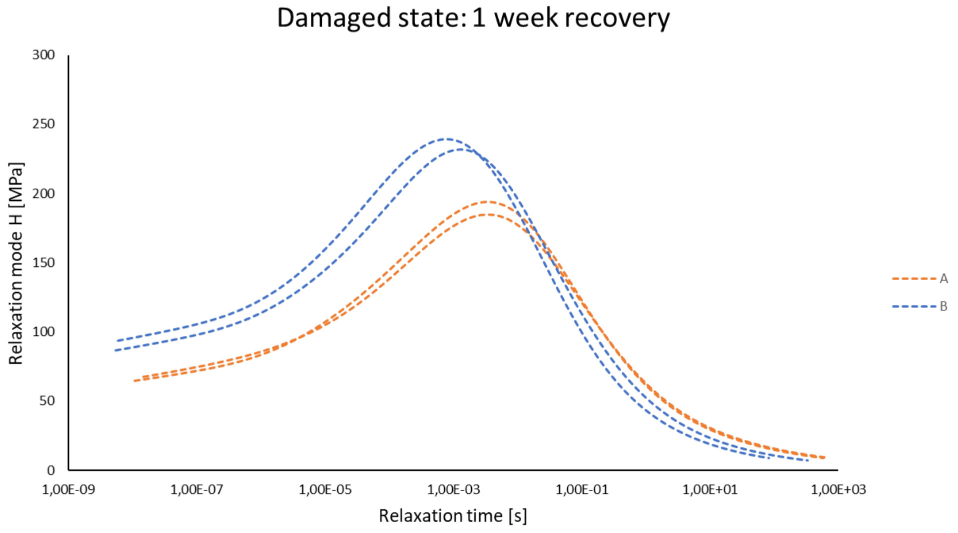

Figure 4.16: CRS obtained from samples tested 1 week after the damage.

Peak height and area under the curve are approximately 20% higher in the specimen from batch B. And in batch A the tendency of the curves to have longer relaxation times is confirmed. However, the results obtained from the various samples are repeatable within the same batch, so the heterogeneity seems to be decreased by the straining in this case as well.

Comparing the average peak values of the whole population with the pristine state (fig. 4.17), the peak height is in line, and the area under the curve is reduced.

The relaxation times without excluding any outliers are generally lower for the damaged specimens.

By looking separately at the two batches, however, the specimens from batch A have a lower average peak height than the pristine state of the same batch, and slightly lower relaxation time and area under the curve. The specimens from batch B on the contrary, show a higher peak height and area under the curve but still a smaller relaxation time than the pristine specimens of the same batch.

4.5.3 Recovery time comparison

A further comparison can be made between the CRS obtained with different recovery time periods (fig. 4.18)): again comparing the average population values, the

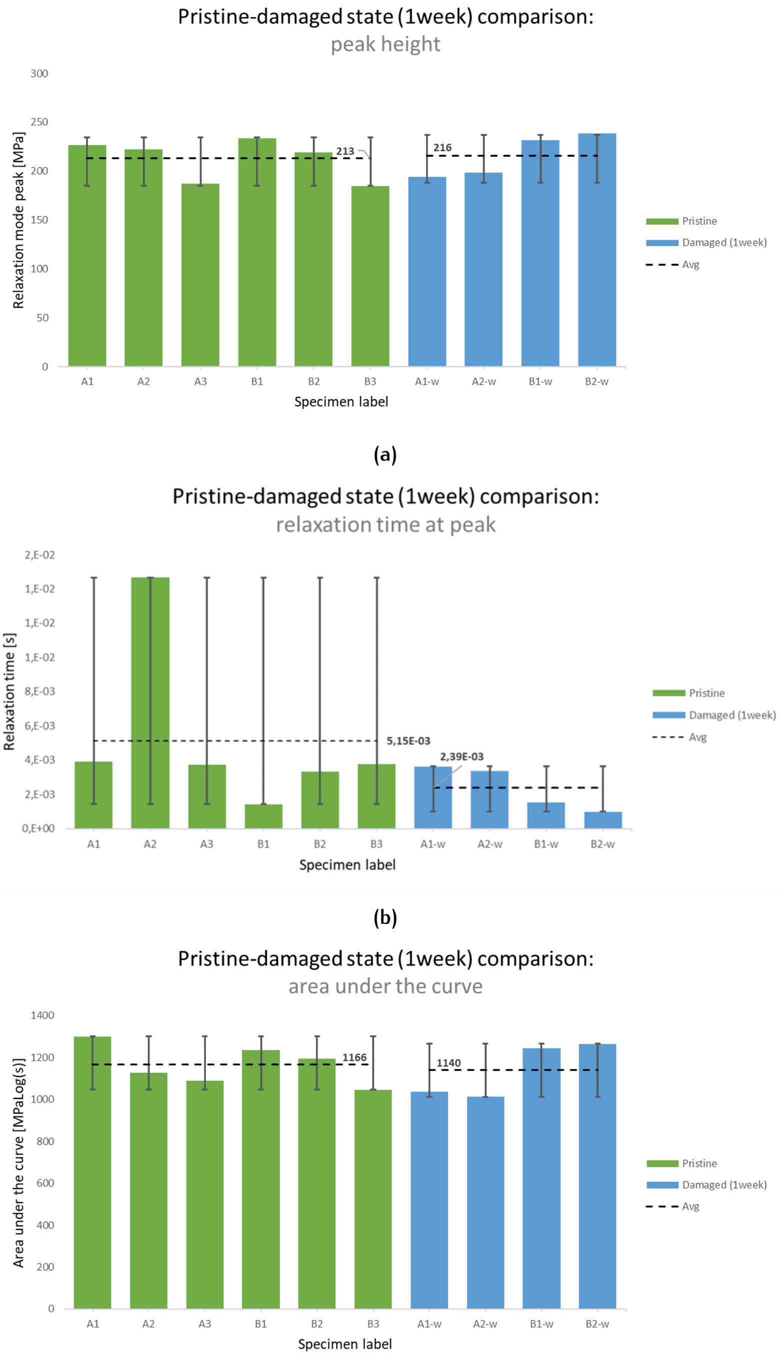

(a)

(b)

(c)

Figure 4.17: Damaged state (1 week) - Pristine state peak parameters: the error bars are associated to the maximum value and minimum value of the considered parameter, the dashed lines represent the mean value. (a) Relaxation mode at the height. (b) Relaxation time at the peak. (c) Total relaxation energy.

peaks appear to be in line and the areas slightly lower for the specimens tested after one week (fig. 4.19). The relaxation times, on the other hand, are longer.

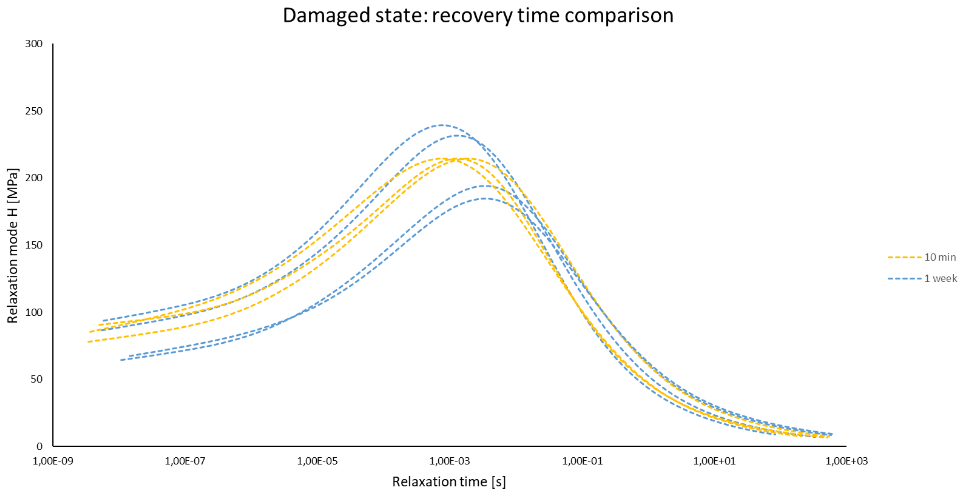

Figure 4.18: CRS obtained from samples tested 10 minutes and 1 week after the damage.

Making the same comparison but considering one batch at a time: batch A shows lower peak and area values and longer relaxation times.

B-w specimens, on the other hand, have slightly higher peak height while area, and relaxation times in line.

Considering the contrasting results, it is difficult to attribute a role to the recovery time after damaging the specimens.

In fact, looking at the specimens from batch A, it would seem that the responses tend toward longer relaxation times and dissipate a smaller amount of energy. In this case, a possible explanation is that a week later, the specimens manage to reduce the strain-induced stress state and to recover a stable equilibrium position, such that they need longer times to relax.

Comparing the specimens from batch B, looking at the peak height it would appear that the captured internal stress state is greater, this is not true looking at the area subtended by the curves, which is approximately equal. The relaxation times also coincide.

Actually, the peak parameters fall within the uncertainty intervals, so the difference in the curves could be explained by the heterogeneity of the samples.

Another possible explanation to justify the different behavior between the two batches, in the specimens tested after one week, is the time passed between the production of the specimens and the actual dynamic test, in which physical aging might have affected: about a month for specimens from batch A (tested on the same day) and 12 and 20 days respectively for specimens B1-w and B2-w from the second batch. But even considering this possibility, a similar trend of the B2-w specimen would have been expected, since it was tested 8 days after the B1-w.

Finally, the effect of the elastic modulus obtained from the stress-strain curves while damaging the samples is investigated.

While for the A-m, B-m samples the elastic modulus found in batch B is 3% higher, in B-w samples is about 9% higher than in A-w. Moreover, the elastic modulus of A-w samples is 2% smaller than the value obtained for the A-m samples and in B-w is 4% higher than in B-m. This could explain the differences in peak height and area under curve observed but actually, is not coherent with the 3% difference found between A-m and B-m. In addition, in Roth's research as well, no trend was found by looking at the Young modulus.

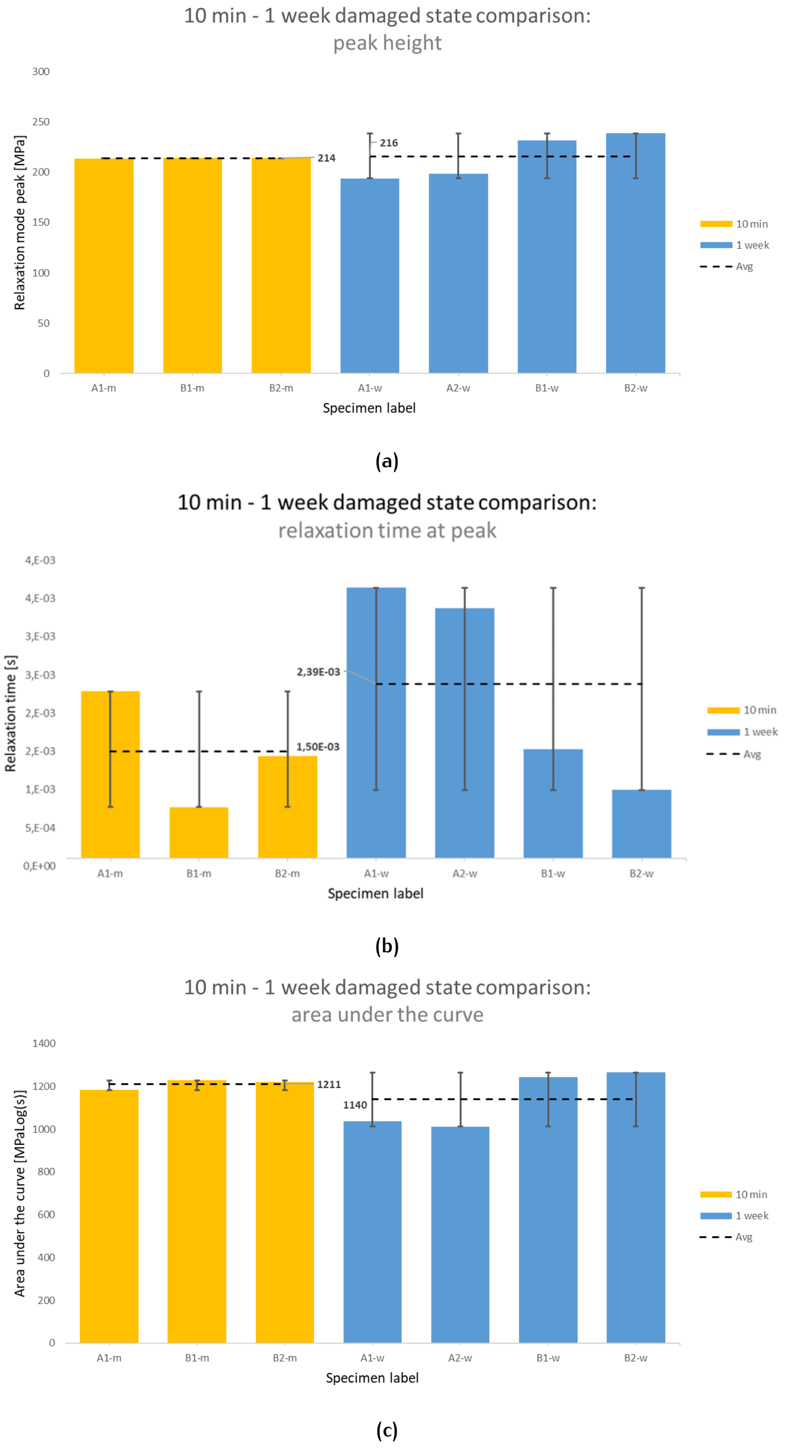

Figure 4.19: Damaged state 10 min - 1 week peak parameters comparison : the error bars are associated to the maximum value and minimum value of the considered parameter, the dashed lines represent the mean value. (a) Relaxation mode at the height. (b) Relaxation time at the peak. (c) Total relaxation energy.

Sample	Young Modulus [MPa]
A-m	4851
B-m	5004
A-w	4762 ± 20
B-w	5198

4.6 OVEN TREATMENT

In the figures 4.20a and 4.20b, the relaxation responses of samples subjected to the oven treatment with subsequent different cooling rates are shown.

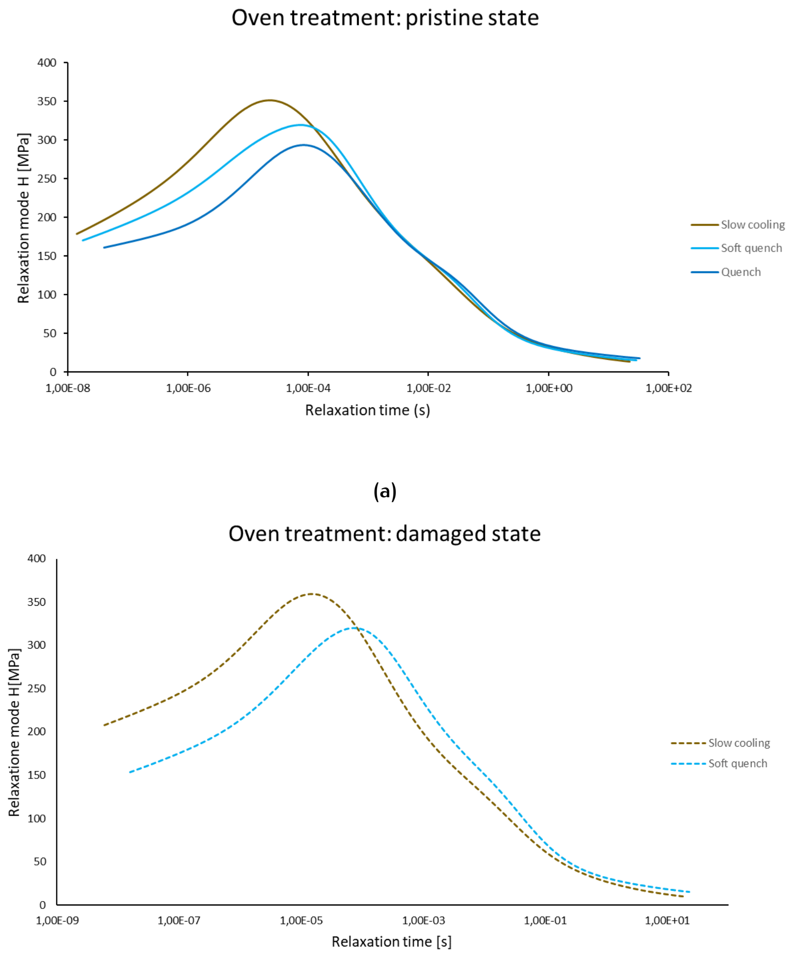

(a)

(b)

Figure 4.20: CRS from samples tested after an oven treatment of 1h at 85°C. (a) pristine state samples, (b) damaged samples.

It is possible to notice that all the curves present a shoulder after the main relaxation peak. This time region, looking at the respective master curves, corresponds to the frequency window in which the data did not obtain a perfect match during the shifting.

In addition, considering the at-shift factor curves (fig.4.21), they are not perfectly linear like the previous tests. This underlines that something at the sample molecular level is changed and the oven treatment is responsible. The temperature at which the samples are heated for 1 hour, indeed, coincides with the temperature in the at-shift factor curve which deviates from linearity.

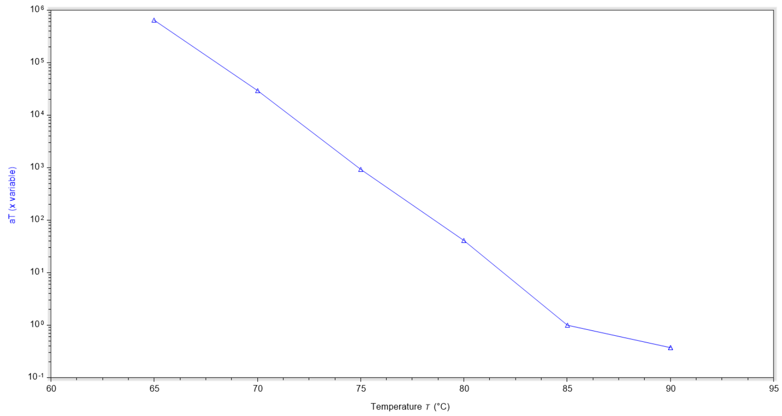

Figure 4.21: Shift factor curve obtained from the rheology data shifting of a sample thermally treated.

It represents the loss modulus peak temperature and it has a physical meaning: larger segments of polymer are able to move cooperatively.

During the treatment, the chain in the polymer network will move, expanding and trying to reach a more suitable equilibrium condition (in every case the motion is limited by junction points and entanglements). The motion will allow the remaining epoxy rings to reach left amines and hence, increase the number of junction points, raising the network's ability to store energy.

Moreover, when the treatment time is over and the oven door is opened, during the first seconds, the temperature of the samples suddenly decreases, stopping network mobility and trapping the network in an unstable equilibrium condition.

For this reason, when the TF sweep test is approaching 85°C the network will release the stress previously trapped modifying the viscoelastic behavior response.

The internal state of stress and the new cross-linking can at the same time, justify the higher peaks and area under the curves obtained in the spectra compared to the results from the pristine samples.

Also, this conclusion is in line with Roth's one: the oven treatment, in that case, was executed at a different temperature ($<$ Tg), at which a minor amount of mobility is allowed and its effect was comparable to an annealing treatment with the only result of decreasing internal stresses.

In this case, the possible annealing effects are erased by the rapid change in temperature.

From the plots in fig. 4.22, it is possible to notice the progressively decreasing peak height and area under the curve and the progressively increasing relaxation time, obtained with a different cooling rate, going from the slow cooling rate to the quench.

Commonly, one would expect to see a different trend, since the quench cooling is expected to entrap a higher state of stress inside the network, showing a major amount of energy to dissipate. But maybe, the key factor is placed in the amount of heat absorbed by the samples and the time they remained at a higher temperature: these factors could have allowed more bonds to be formed, increasing the storable energy. It is possible to assess this by comparing the temperature profiles obtained by plotting temperature of the samples, collected during the cooling, versus time (fig. 4.24).

Damaged thermally treated samples show the same trend previously discussed. Comparing them to the pristine ones, about the same values of peak height and area under the curve are found, and a higher difference is found between the relaxation time of the samples subjected to the slow cooling process (fig. 4.23). Heat treatment has a homogenising effect on the specimens, helping to reduce the differences found earlier between the pristine and damaged state specimens.

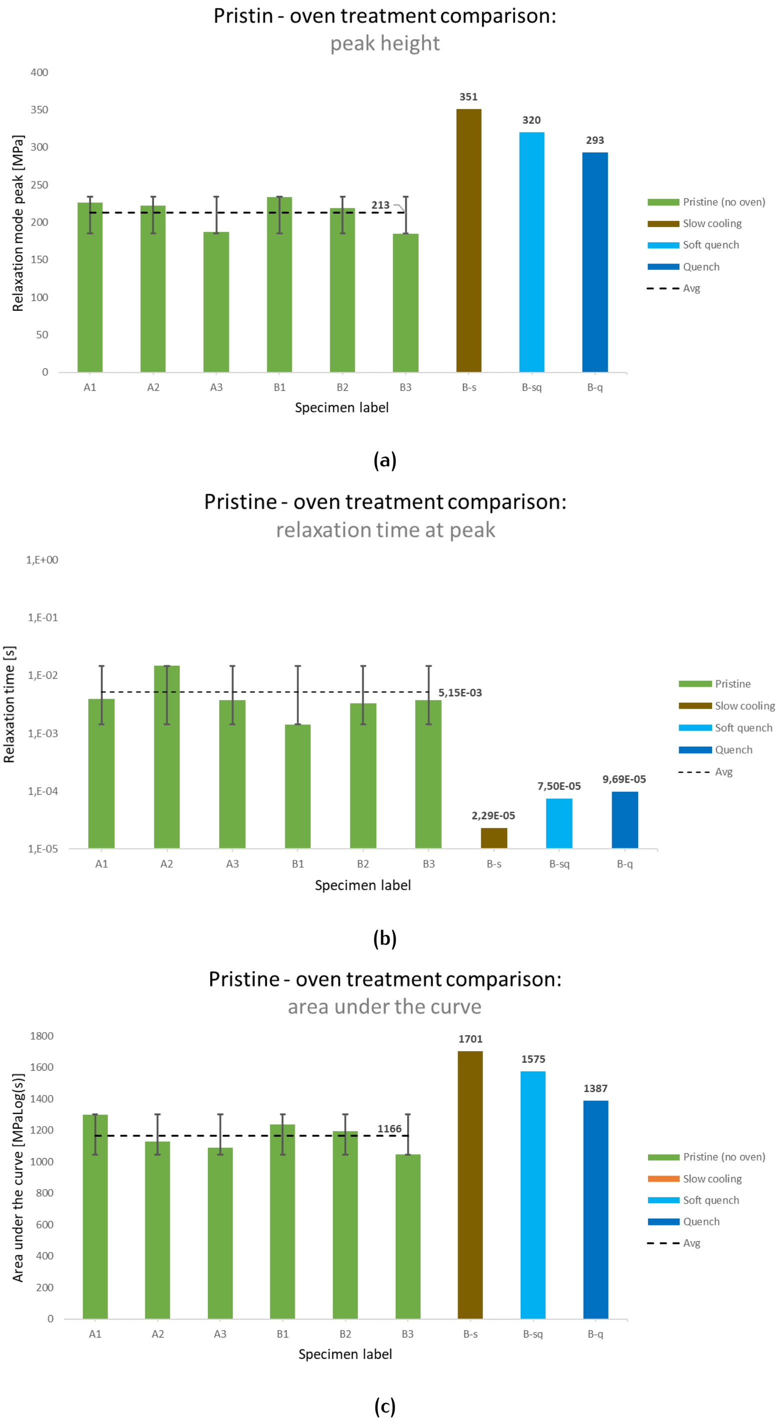

(a)

(b)

(c)

Figure 4.22: Pristine state - Oven treatment peak parameters comparison : the error bars are associated to the maximum value and minimum value of the considered parameter, the dashed lines represent the mean value. (a) Relaxation mode at the height. (b) Relaxation time at the peak. (c) Total relaxation energy.

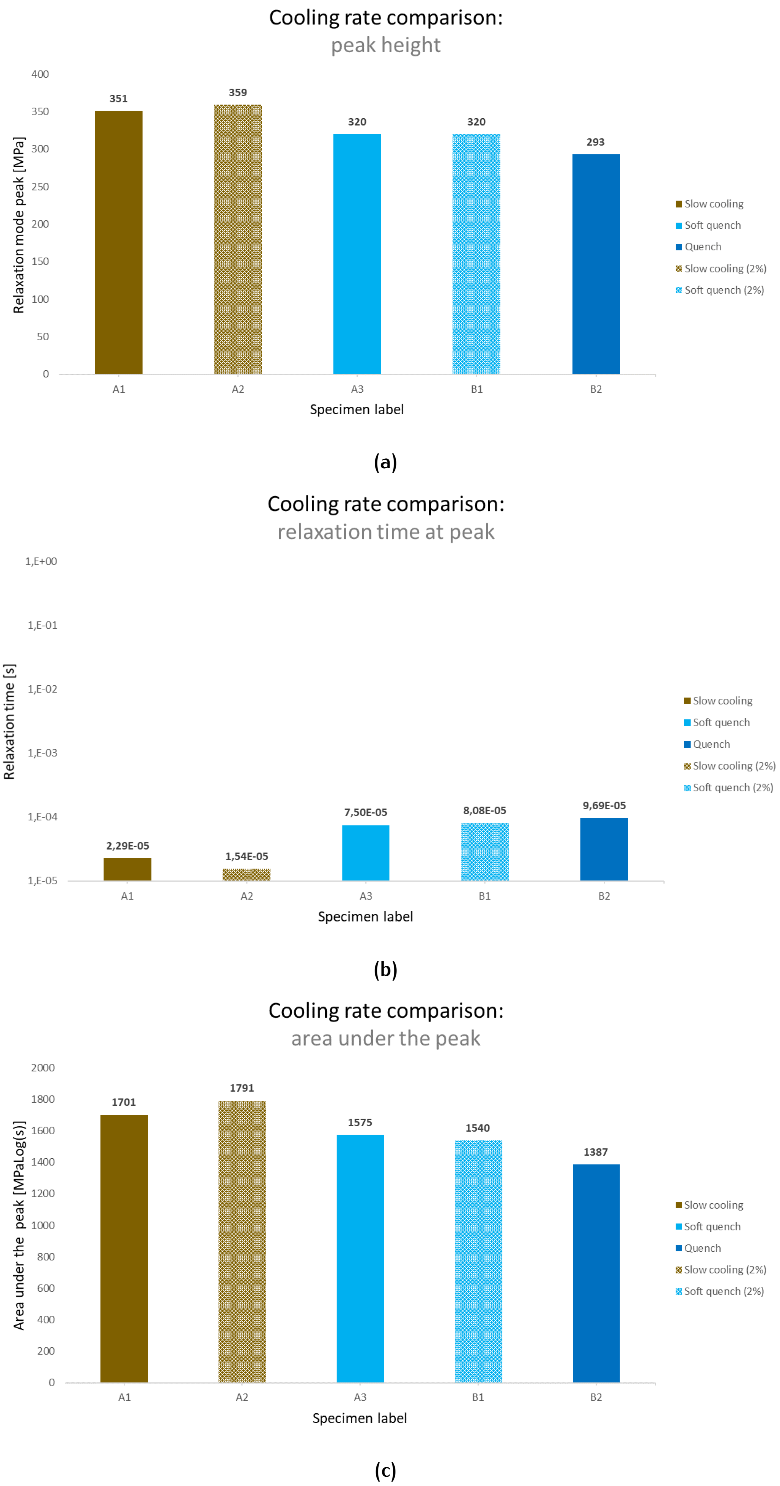

(a)

(b)

(c)

Figure 4.23: Pristine state - Damaged state after the oven treatment peak parameters comparison : the error bars are associated to the maximum value and minimum value of the considered parameter, the dashed lines represent the mean value. (a) Relaxation mode at the height. (b) Relaxation time at the peak. (c) Total relaxation energy.

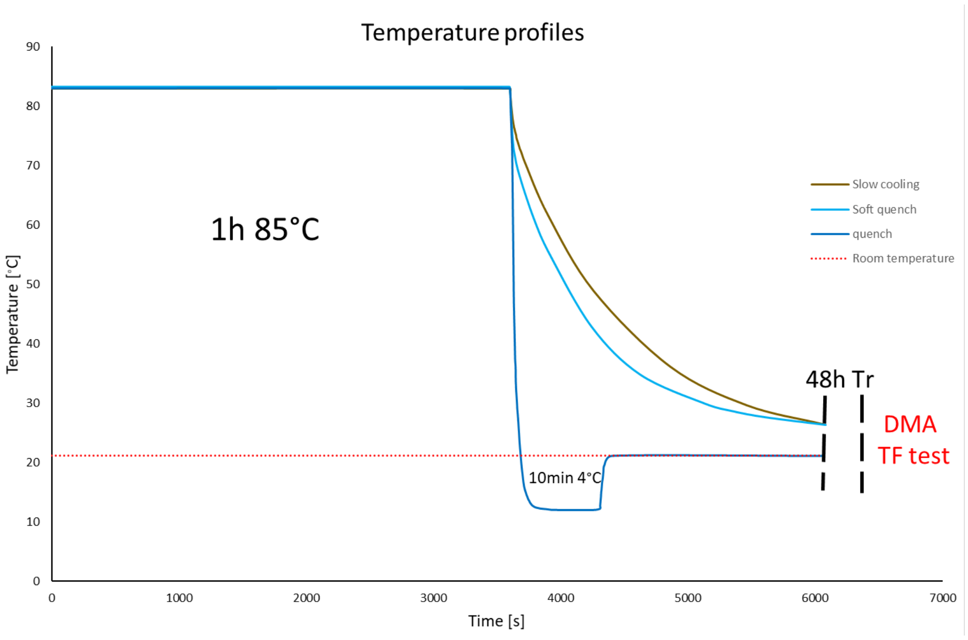

Figure 4.24: Temperature data versus time collected during the three different cooling mechanisms.

5 DISCUSSION AND CONCLUSIONS

5.1 PRISTINE STATE

By looking at the pristine samples, one is able to certify the capability and sensibility of the technique to recognize samples heterogeneity and is possible to identify an uncertainty range related to the peak parameters: ($\Delta_{peakheight}$: $50Mpa$, $\Delta_{relaxationtime}$: $1,3x10^{-2}s$ and Δ_{area} : $255MpaLog(s)$).

There are different ways of considering heterogeneity: for instance, at a very small scale level, it can be considered as chemical in-homogeneity but, another way is considering the not homogeneous spatial distribution of cross-links that can affect the distribution of network-strand lengths. The latter, has as a consequence a different distribution of polymer mesh size.

In addition, most polymer networks display topological and connectivity defects such as dangling chain ends, chains forming closed loops, and crosslinker–crosslinker shortcuts [36] .

All these features are strongly related to the polymer's ability to store energy.

Among these factors, it should be mentioned the internal state of stress, influenced by both the curing progress, if unreacted groups remain, and the state of stress generated when the mold is removed from the oven after the curing. The latter can cause in the samples different internal stress state, since the bottom part of the specimen is in contact with the hot mold (tensile state), while the surface is exposed to the air at room temperature (compressive state) [37].

Since below Tg, the polymer is not in equilibrium and a certain amount of entropy is 'frozen in' as a consequence of the loss of chain mobility [38], aging can occur, by driving the material closer to equilibrium and contributing to stress relaxation.

All these factors could have affected the elastic behavior and so the amount of storable energy, influencing CRS responses.

Samples (from a single batch) have been tested for a period of time that covers a month and different states of equilibrium could have been captured while testing them with the DMA.

Even if a correlation between the test dates and results has not been found, time influence is not excluded, if considered in a combination with other heterogeneity factors. Furthermore, the samples in which greater heterogeneity (pristine) is found are those tested a few days after production, probably when the network is subject to a higher ageing rate.

To better understand the correlation between polymer network and its dynamic behavior, spectroscopy tests and techniques such as scattering and MQ-NMR , could be helpful to check chemical composition and defects presence, before the execution of the relaxation protocol.

5.2 DAMAGED STATE

In the damaged samples tested after 10 minutes, the values of the peak parameters are in line with those of the pristine state or at least within the uncertainty range except for the relaxation times, which are lower in the deformed state.

In the specimens tested after one week, a distinction must be made between the two batches because they show two different behaviors. Compared with the pristine ones, both batches show smaller relaxation times, but in the specimens from batch A, the modulus values at the peak and areas are smaller while in B, roughly the same.

Compared to the specimens tested after 10 minutes, batch A shows smaller peaks and areas but longer relaxation times, instead, batch B has bigger areas and peaks and approximately the same relaxation times.

It is not possible to derive an accurate trend of the expected recovery time because is first necessary to understand which is the cause of the differences between the two batches.

5.2.1 Relaxation time

The most important indications about the damaged state, are the reduced heterogeneity in the results obtained from samples belonging to the same batch and the shorter relaxation times compared with the pristine state.

The time trend could have 3 meanings:

- effect due to the damage, but the opposite behavior was expected since fewer bonds contribute to the elastic response;
- effect due to the stress state induced by the deformation, and thus the need to recover an equilibrium position;
- effect due to a higher percentage of crosslinks present in the specimens: if the curing process has continued, more bonds give the network more incentive to relax.

5.3 OVEN TREATMENT

More consistent results are obtained from heat-treated specimens where a trend can be discerned: the energy dissipated is progressively greater in specimens that remain for longer at a high T and the relaxation times are progressively shorter. But again it is not possible to recognize the strain by analyzing the peak parameters considered.

It is interesting to note that the thermal energy absorbed by the specimens has a greater influence on the storable energy than the internal stresses captured by subjecting the specimens to different degrees of cooling.

Also in this case the heterogeneity of the samples decreases.

5.4 CONCLUSION

The purpose of this work was using the Continuous relaxation spectrum to recognize an internal damage state in epoxy-amine samples damaged inducing plastic strain via tensile test.

The main differences found between the pristine and the damaged state concern the samples heterogeneity, decreased in the latter, and the relaxation time, shorter in the damaged state. It was not possible to find other trends looking at the other peak parameters considered.

The recovery time after the straining step affects the CRS but a trend is not been found since the two batches tested after 1 week showed opposite behaviours.

The oven treatment contributes to decrease the heterogeneity and the cooling rate strongly affects the relaxation response.

To obtain more comparable results, for the next experiments, one recommendation is to perform the tests when the specimens are more stabilized after the cure, or considering to add another post-cure step (since the percentage of the cross-links seems to increase in the thermally treated specimens). In any case is better to perform all the tests in a narrow period of time to avoid that aging, humidity and exposure to light may affect the results.

An oven treatment is also suggested with the purpose of decreasing the starting heterogeneity and for the same purpose it would be of great importance to test samples obtained from a single batch.

It should be taken into account that after straining the samples beyond the yield point, in this case, 2%, the elastic part of straining will be recovered once the load is released, so the effective permanent damage is much smaller. To distinguish its effect from experimental error and deviation of the results due to network heterogeneity, would be important using the protocol on a polymer with a broader plastic field.

Another solution could be to find other curve parameters to analyze or deconvolute the spectrum.

A different way to see the spectrum, using the TTS principle, exists. The data present at low (high) relaxation times correspond to the data collected at high (low) frequencies in the master curve. The region at high frequencies corresponds in turn to testing the specimen in a low-temperature range and in particular lower than Tg. For this reason, is possible to recognize in the CRS the three characteristic zones of viscoelastic behavior: the glassy region, the transition region, and the rubbery plateau.

In the viscous region having already passed the alpha transition, it is less probable to find clues about the state of damage. Instead, it would be useful to find characteristic parameters of the curve in the pre-peak region.

BIBLIOGRAPHY

[1] Jean Lemaitre. *A Course on Damage Mechanics*. Second Revised and Enlarged Edition. Berlin, Heidelberg: Springer Berlin Heidelberg, 1996. ISBN: 3642182569 (cit. on p. 1).

[2] Martin D. Hager, Peter Greil, Christoph Leyens, Sybrand van der Zwaag, and Ulrich S. Schubert. "Self-Healing Materials". In: *Advanced Materials* 22.47 (2010), pp. 5424–5430. DOI: https://doi.org/10.1002/adma.201003036. eprint: https://onlinelibrary.wiley.com/doi/pdf/10.1002/adma.201003036. URL: https://onlinelibrary.wiley.com/doi/abs/10.1002/adma.201003036 (cit. on p. 1).

[3] Judit Canadell, Han Goossens, and Bert Klumperman. "Self-Healing Materials Based on Disulfide Links". In: *Macromolecules* 44.8 (2011), pp. 2536–2541. DOI: 10.1021/ma2001492. eprint: https://doi.org/10.1021/ma2001492. URL: https://doi.org/10.1021/ma2001492 (cit. on p. 1).

[4] Ying-Ling Liu and Tsai-Wei Chuo. "Self-healing polymers based on thermally reversible Diels–Alder chemistry". In: *Polym. Chem.* 4 (7 2013), pp. 2194–2205. DOI: 10.1039/C2PY20957H. URL: http://dx.doi.org/10.1039/C2PY20957H (cit. on p. 1).

[5] P. Cordier, F. Tournilhac, C. Soulié-Ziakovic, and L. Leibler. *Self-healing and thermoreversible rubber from supramolecular assembly*. Vol. 451. 7181. 2008, pp. 977–80. DOI: doi:10.1038/nature06669 (cit. on p. 1).

[6] Stefan Bode, Linda Zedler, Felix H. Schacher, Benjamin Dietzek, Michael Schmitt, Jürgen Popp, Martin D. Hager, and Ulrich S. Schubert. "Self-Healing Polymer Coatings Based on Crosslinked Metallosupramolecular Copolymers". In: *Advanced Materials* 25.11 (2013), pp. 1634–1638. DOI: https://doi.org/10.1002/adma.201203865 (cit. on p. 1).

[7] S. van der Zwaag, A.M. Grande, W. Post, S.J. Garcia, and Teunis Cornelis Bor. "Review of current strategies to induce self-healing behaviour in fibre reinforced polymer based composites". English. In: *Materials science and technology* 30.13 (2014). Special issue on Smart materials, pp. 1633–1641. ISSN: 0267-0836. DOI: 10.1179/1743284714Y.0000000624 (cit. on p. 1).

[8] Zhong Nan and Post Wouter. "Self-repair of structural and functional composites with intrinsically self-healing polymer matrices: A review". In: *Composites Part A: Applied Science and Manufacturing* 69 (2015), pp. 226–239. ISSN: 1359-835X. DOI: https://doi.org/10.1016/j.compositesa.2014.11.028 (cit. on p. 1).

[9] Zhang Zhenhui, Hu Yuling, Liu Zhengsheng, and Guo Tianying. "Synthesis and evaluation of a moisture-promoted healing copolymer". In: *Polymer* 53.14 (2012), pp. 2979–2990. ISSN: 0032-3861. DOI: https://doi.org/10.1016/j.polymer.2012.04.048. URL: https://www.sciencedirect.com/science/article/pii/S0032386112003795 (cit. on p. 1).

[10] Ying Yang and Marek W. Urban. "Self-healing polymeric materials". In: *Chem. Soc. Rev.* 42 (17 2013), pp. 7446–7467. DOI: 10.1039/C3CS60109A. URL: http://dx.doi.org/10.1039/C3CS60109A (cit. on p. 2).

[11] Seon-Mi Kim, Hyeonyeol Jeon, Sung-Ho Shin, Seul-A Park, Jonggeon Jegal, Sung Yeon Hwang, Dongyeop X. Oh, and Jeyoung Park. "Superior Toughness and Fast Self-Healing at Room Temperature Engineered by Transparent Elastomers". In: *Advanced Materials* 30.1 (2018), p. 1705145. DOI: https://doi.org/10.1002/adma.201705145 (cit. on p. 2).

[12] Yue Lai, Xiao Kuang, Ping Zhu, Miaoming Huang, Xia Dong, and Dujin Wang. "Colorless, Transparent, Robust, and Fast Scratch-Self-Healing Elastomers via a Phase-Locked Dynamic Bonds Design". In: *Advanced Materials* 30.38 (2018), p. 1802556. DOI: https://doi.org/10.1002/adma.201802556 (cit. on p. 2).

[13] Post Wouter, Ranjita K. Bose, Santiago J. García, and Sybrand Van Der Zwaag. "Healing of early stage fatigue damage in ionomer/Fe3O4 nanoparticle composites". English. In: *Polymers* 8.12 (Dec. 2016). ISSN: 2073-4360. DOI: 10.3390/polym8120436 (cit. on p. 2).

[14] M. Hernández, A.M. Grande, S. van der Zwaag, and S.J. García. "Monitoring Network and Interfacial Healing Processes by Broadband Dielectric Spectroscopy: A Case Study on Natural Rubber". In: *ACS Applied Materials & Interfaces* 8.16 (2016), pp. 10647–10656. DOI: 10.1021/acsami.6b02259. URL: https://doi.org/10.1021/acsami.6b02259 (cit. on p. 2).

[15] Roth Caspar. "An investigation into the relaxation response of a self-healing dual network polymer through controlled introduction of strain damage". Master thesis. Delft University of Technology, Aug. 2021 (cit. on pp. 2, 18).

[16] Babaei Behzad, Davarian Ali, Pryse Kenneth M., Elson Elliot L., and Genin Guy M. "Efficient and optimized identification of generalized Maxwell viscoelastic relaxation spectra". In: *Journal of the Mechanical Behavior of Biomedical Materials* 55 (2016), pp. 32–41. DOI: https://doi.org/10.1016/j.jmbbm.2015.10.008. URL: https://www.sciencedirect.com/science/article/pii/S1751616115003811 (cit. on p. 5).

[17] Mathieu Verdet, Alexander Salenikovich, Alain Cointe, Jean-Luc Coureau, Philippe Galimard, William Toro, Pierre Blanchet, and Christine Délisée. "Mechanical Performance of Polyurethane and Epoxy Adhesives in Connections with Glued-in Rods at Elevated Temperatures". In: *BioRessources* 11 (Aug. 2016), pp. 8200–8214. DOI: 10.15376/biores.11.4.8200-8214 (cit. on p. 5).

[18] Ankiewicz Scott, Orbey Nese, Watanabe Hiroshi, Lentzakis Helen, and Dealy John M. "On the use of continuous relaxation spectra to characterize model polymers". In: *Journal of Rheology* 60 (2016), pp. 1115–1120 (cit. on pp. 5, 6, 8).

[19] Fei Zhang, Lan Wang, Chao Li, and Yongming Xing. "The Discrete and Continuous Retardation and Relaxation Spectrum Method for Viscoelastic Characterization of Warm Mix Crumb Rubber-Modified Asphalt Mixtures". In: *Materials* 13 (Aug. 2020), p. 3723. DOI: 10.3390/ma13173723 (cit. on p. 5).

[20] Zienkiewicz O.C., Taylor R.L., and Fox David. "Chapter 1 - General Problems in Solid Mechanics and Nonlinearity". In: *The Finite Element Method for Solid and Structural Mechanics (Seventh Edition)*. Ed. by O.C. Zienkiewicz, R.L. Taylor, and David Fox. Seventh Edition. Oxford: Butterworth-Heinemann, 2014, pp. 1–20. DOI: https://doi.org/10.1016/B978-1-85617-634-7.00001-6 (cit. on p. 5).

[21] Volkan Yesilyurt, Andrew M. Ayoob, Eric A. Appel, Jeffrey T. Borenstein, Robert Langer, and Daniel G. Anderson. "Mixed Reversible Covalent Crosslink Kinetics Enable Precise, Hierarchical Mechanical Tuning of Hydrogel Networks". In: *Advanced Materials* 29.19 (2017), p. 1605947. DOI: https://doi.org/10.1002/adma.201605947 (cit. on p. 5).

[22] Evagelia Kontou. "Relaxation time spectra of linear and crosslinked polymers". In: *Journal of Applied Polymer Science* 67 (Jan. 1998), pp. 679–684. DOI: 10.1002/(sici)1097-4628(19980124)67:4⟨679::aid-app10⟩3.0.co;2-n (cit. on p. 5).

[23] Josef Honerkamp and Jürgen Weese. "A nonlinear regularization method for the calculation of relaxation spectra". In: *Rheologica Acta* 32 (1993), pp. 65–73 (cit. on pp. 5, 8).

[24] Montano Vincenzo, Stephen J. Picken, Sybrand Van Der Zwaag, and Santiago J. Garcia. “A deconvolution protocol of the mechanical relaxation spectrum to identify and quantify individual polymer feature contributions to self-healing”. English. In: *Physical chemistry chemical physics (PCCP)* 21.19 (2019), pp. 10171–10184. ISSN: 1463-9076. DOI: 10.1039/c9cp00417c (cit. on pp. 6, 18).

[25] Kwang Soo Cho. “Time-Temperature Superposition”. In: *Viscoelasticity of Polymers: Theory and Numerical Algorithms*. Dordrecht: Springer Netherlands, 2016, pp. 437–457. ISBN: 978-94-017-7564-9. DOI: 10.1007/978-94-017-7564-9_8. URL: https://doi.org/10.1007/978-94-017-7564-9_8 (cit. on p. 7).

[26] Williams Malcolm L., Landel Robert F., and Ferry John D. “The Temperature Dependence of Relaxation Mechanisms in Amorphous Polymers and Other Glass-Forming Liquids”. In: *Journal of the American Chemical Society* 77 (1955), pp. 3701–3707 (cit. on p. 7).

[27] Liviu-Iulian Palade, Hans J. Lehermeier, and John R. Dorgan. “Melt Rheology of High l-Content Poly(lactic acid)”. In: *Macromolecules* 34.5 (2001), pp. 1384–1390. DOI: 10.1021/ma001173b. URL: https://doi.org/10.1021/ma001173b (cit. on p. 8).

[28] William Pinto Hernández, Daniel Castello, N. Roitman, and Carlos Magluta. “Thermorheologically simple materials: A bayesian framework for model calibration and validation”. In: *Journal of Sound and Vibration* 402 (Aug. 2017), pp. 14–30. DOI: 10.1016/j.jsv.2017.05.005 (cit. on p. 8).

[29] Keith M. Kirkwood, L. Gary Leal, Dimitris Vlassopoulos, Paraskevi Driva, and Nikos Hadjichristidis. “Stress Relaxation of Comb Polymers with Short Branches”. In: *Macromolecules* 42.24 (2009), pp. 9592–9608. DOI: 10.1021/ma900950s. URL: https://doi.org/10.1021/ma900950s (cit. on p. 8).

[30] M. Kapnistos, D. Vlassopoulos, J. Roovers, and L. G. Leal. “Linear Rheology of Architecturally Complex Macromolecules: Comb Polymers with Linear Backbones”. In: *Macromolecules* 38.18 (2005), pp. 7852–7862. DOI: 10.1021/ma050644x. URL: https://doi.org/10.1021/ma050644x (cit. on p. 8).

[31] Ferry J. *Viscoelastic properties of polymers*. 3rd. John Wiley and Sons, 1980 (cit. on p. 9).

[32] Singh Amit Kumar, Panda Bishnu Prasad, Mohanty Smita, Nayak Sanjay Kumar, and Gupta Manoj Kumar. “Thermokinetics behavior of epoxy adhesive reinforced with low viscous aliphatic reactive diluent and nano-fillers”. In: *Korean Journal of Chemical Engineering* (Sept. 2017). DOI: 10.1007/s11814-017-0221-z (cit. on p. 11).

[33] Wiltink Anniek. “Evaluation of Polymer Relaxation Dynamics: Using Laser Speckle Imaging and Dynamic Mechanical Analysis”. Master thesis. Delft University of Technology, Sept. 2021 (cit. on pp. 12, 18).

[34] Jyotishkumar Parameswaranpillai, Jürgen Pionteck, Rüdiger Hässler, Sajeev George, Uroš Cvelbar, and Sabu Thomas. “Studies on Stress Relaxation and Thermomechanical Properties of Poly(acrylonitrile-butadiene-styrene) Modified EpoxyAmine Systems”. In: *Industrial & Engineering Chemistry Research* 50 (Mar. 2011), pp. 4432–4440. DOI: 10.1021/ie1016915 (cit. on p. 18).

[35] Brad H. Jones, David R. Wheeler, Hayden T. Black, Mark E. Stavig, Patricia S. Sawyer, Nicholas H. Giron, Mathias C. Celina, Timothy N. Lambert, and Todd M. Alam. “Stress Relaxation in Epoxy Thermosets via a Ferrocene-Based Amine Curing Agent”. In: *Macromolecules* 50.13 (2017), pp. 5014–5024. DOI: 10.1021/acs.macromol.7b00501 (cit. on p. 18).

[36] F Di Lorenzo and S. Seiffert. “Nanostructural heterogeneity in polymer networks and gels”. In: *Polym.Chem.* 6 (2015), pp. 5515–5528. DOI: 10.1039/C4PY01677G (cit. on p. 37).

[37] Jim R. White. "Polymer ageing: physics, chemistry or engineering? Time to reflect". In: *Comptes Rendus Chimie* 9 (2006), pp. 1396–1408. DOI: 10.1016/j.crci.2006.07.008. (cit. on p. 37).

[38] N. Tschoegl, W.G. Knauss, and I. Emri. "The Effect of Temperature and Pressure on the Mechanical Properties of Thermo- and/or Piezorheologically Simple Polymeric Materials in Thermodynamic Equilibrium – A Critical Review". In: *Mechanics of Time-Dependent Materials* 6 (2002), pp. 53–99. DOI: 10.1023/A:1014421519100 (cit. on p. 37).

A APPENDIX

A.1 THERMAL CHARACTERIZATION

A.1.1 TGA results

Temperature sweep tests are conducted on a Perkin Elmer TGA 4000, from 20°C to 500°C, to verify the thermal stability of the polymer. The heating rate used is 10°C/min. The tests are executed in a Nitrogen controlled environment.

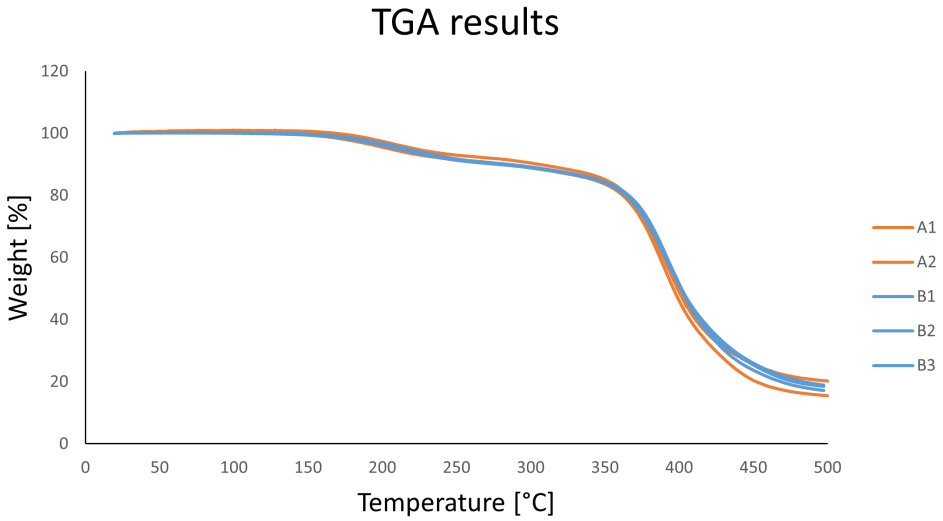

Figure A.1: TGA results: five samples in total tested from the two batches. The strarting weight is within 4-8mg. The tests are conducted on a Perkin Elmer TGA 4000, from 20°C to 500°C, with a heating rae of 10°C/min.

A.1.2 DSC results

The following graph report the results obtained from the temperature ramp tests executed on a TA instrument DSC250 machine. The tests started from 0°C and reached 140°C. Two heating ramps under Nitrogen are run with a 10°C/min rate, separated by a cooling ramp with a 5°C/min rate. The glass transition temperature (Tg) is taken from the second heating ramp and it is selected as the midpoint of the endothermic event.

The same test is executed on a sample after the execution of a TF sweep test and after the oven treatment.

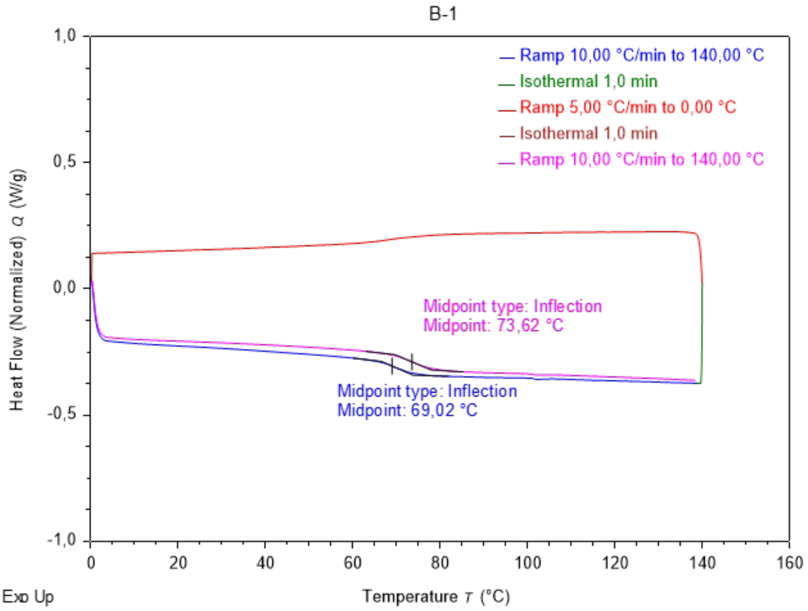

Figure A.2: DSC results: sample B1.

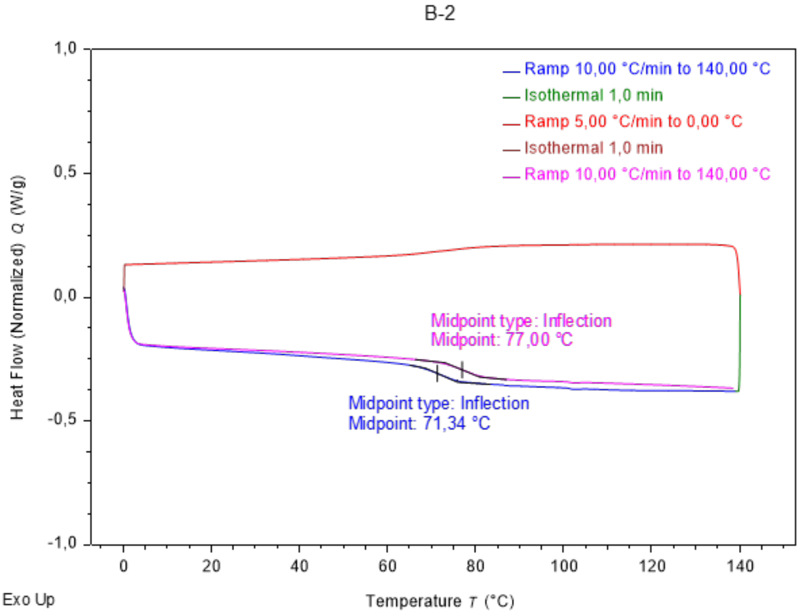

Figure A.3: DSC results: sample B2.

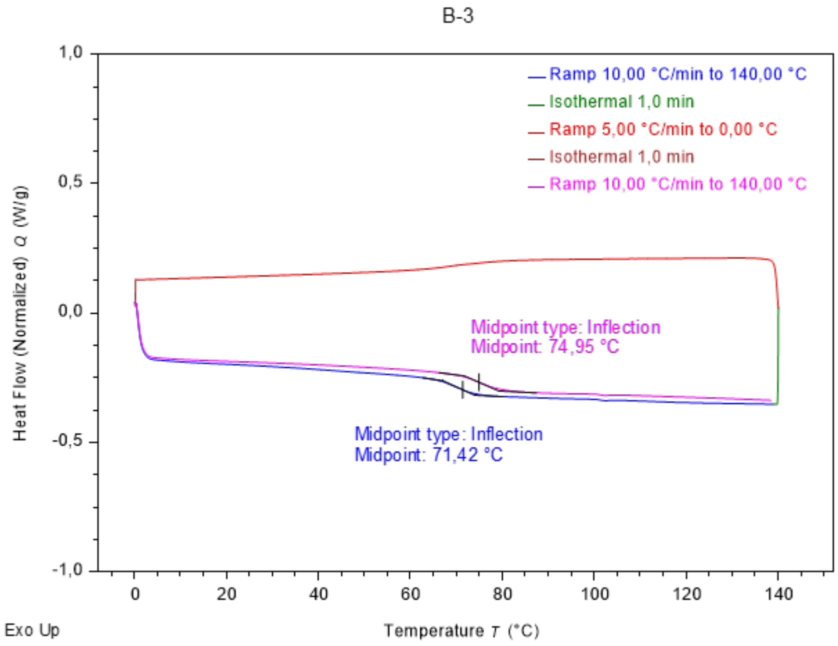

Figure A.4: DSC results: sample B3.

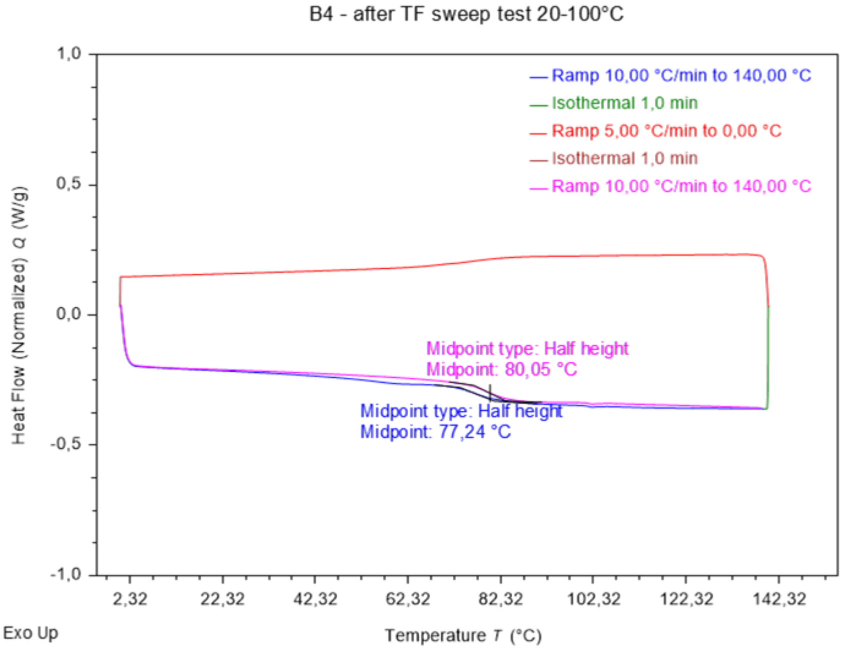

Figure A.5: DSC results: sample B4 after the TF sweep test.

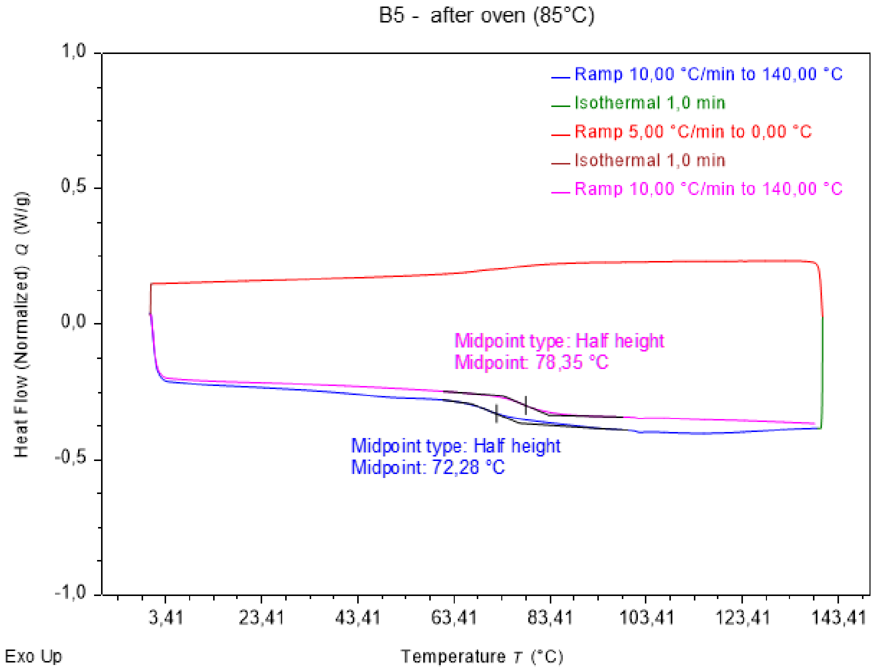

Figure A.6: DSC results: sample B5 after the oven treatment.

A.2 DMA RESULTS

A.2.1 Amplitude sweep

Two amplitude sweep tests were executed to verify the linear viscoelastic range, at the temperature of 20°C and 120°C with a frequency of 1Hz. The logarithmic strain sweep is performed from 0.01 to 1.0%.

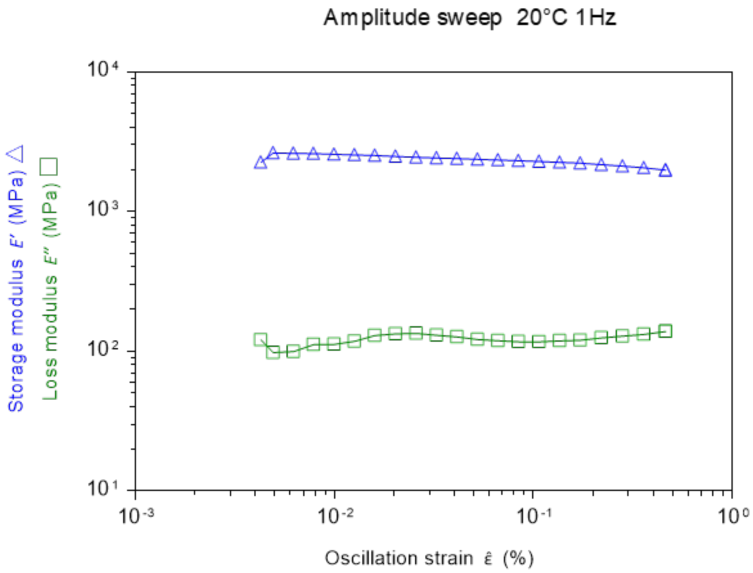

Figure A.7: Amplitude sweep results at 20°C.

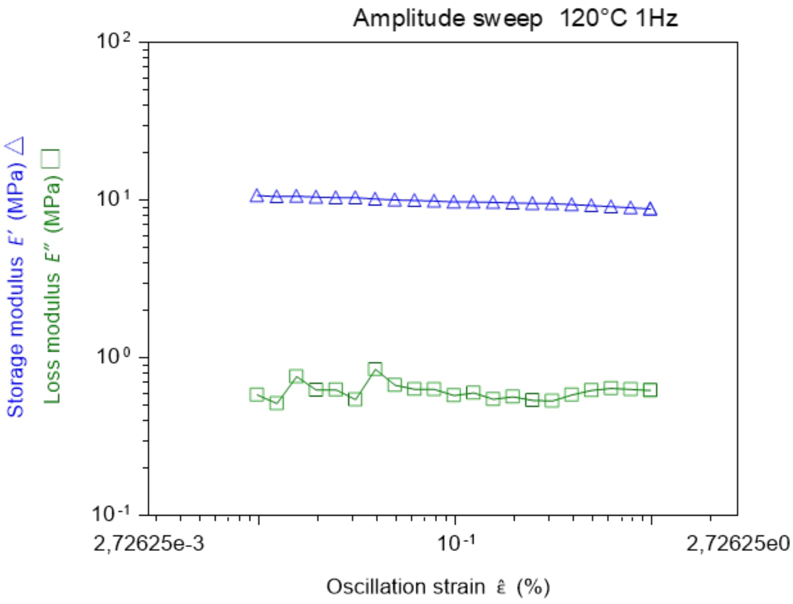

Figure A.8: Amplitude sweep results at 120°C.

A.2.2 TTS master curve

The following graphs report the TTS master curves and the respective aT shift factor plot obtained for the pristine, damaged state and thermally treated samples.

The curves are obtained by shifting the storage and loss moduli data collected between 65°C and 90°C using the WLF model. The reference temperature selected is 85°C.

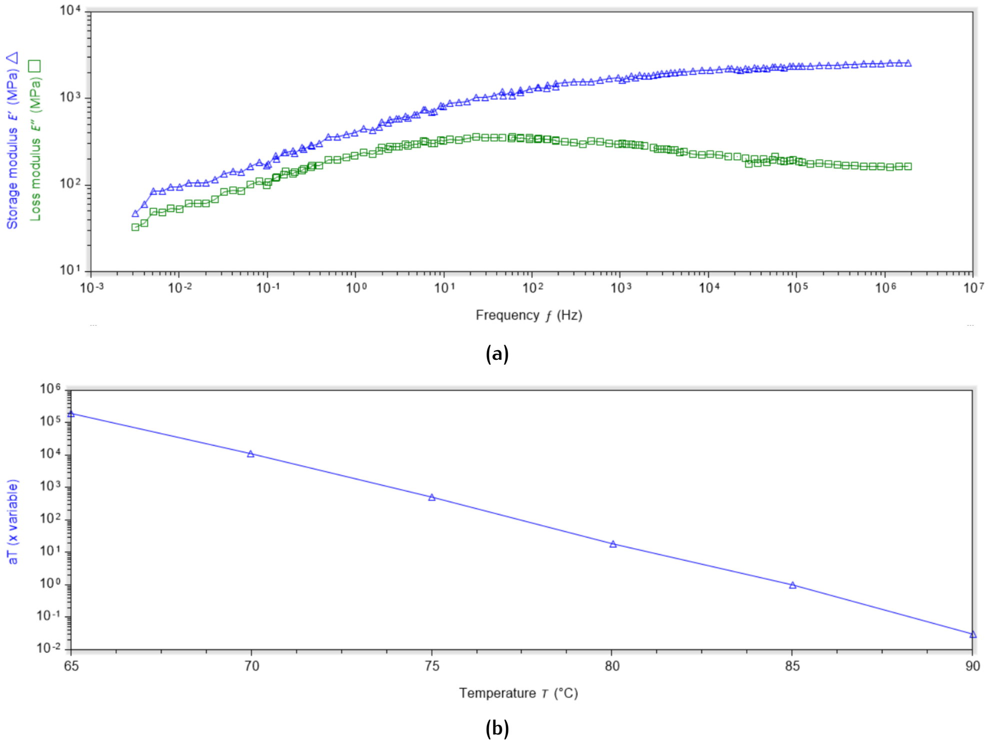

Figure A.9: Reduced TTS master curve and horizontal shift factors aT for: A1 (pristine state). Tref = 85°C

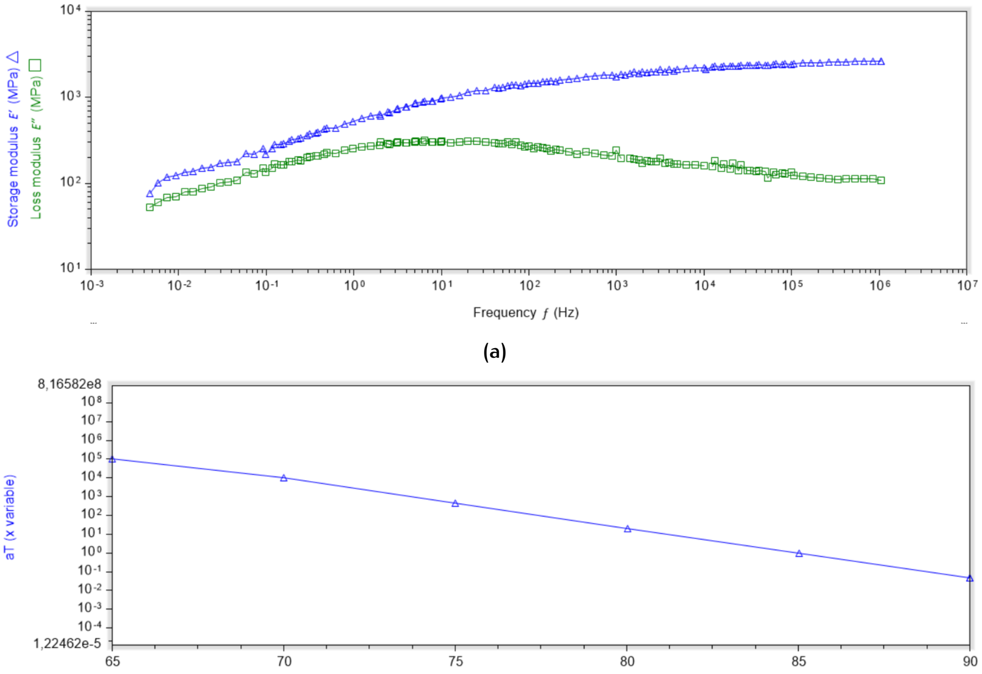

(a)

(b)

Figure A.10: Reduced TTS master curve and horizontal shift factors aT for: A2 (pristine state). Tref = 85°C

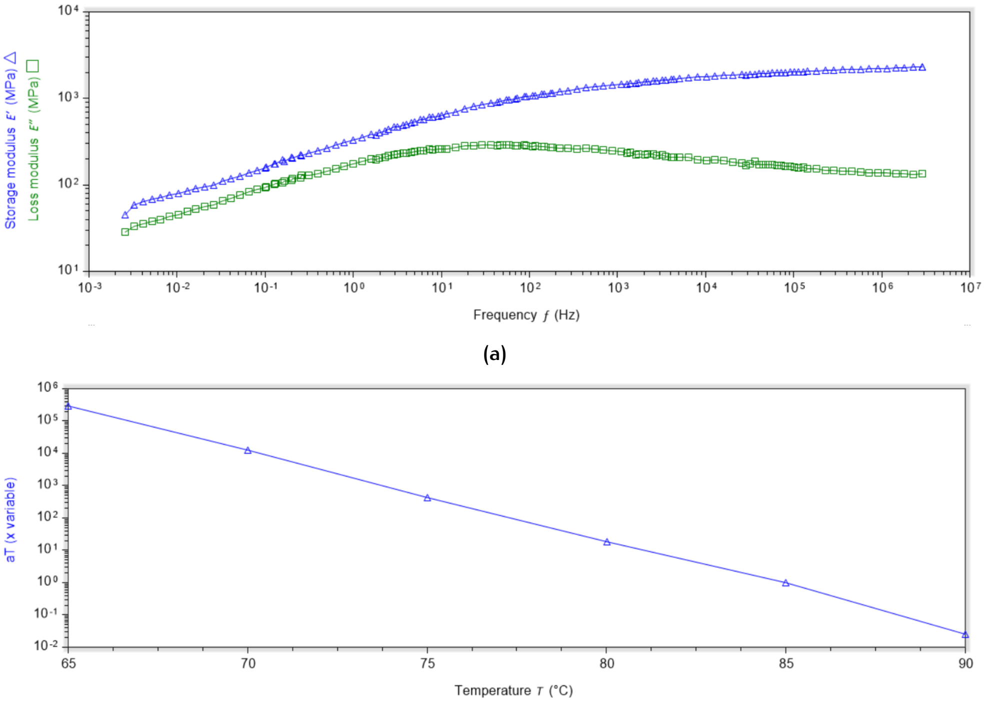

(a)

(b)

Figure A.11: Reduced TTS master curve and horizontal shift factors aT for: A3 (pristine state). Tref = 85°C

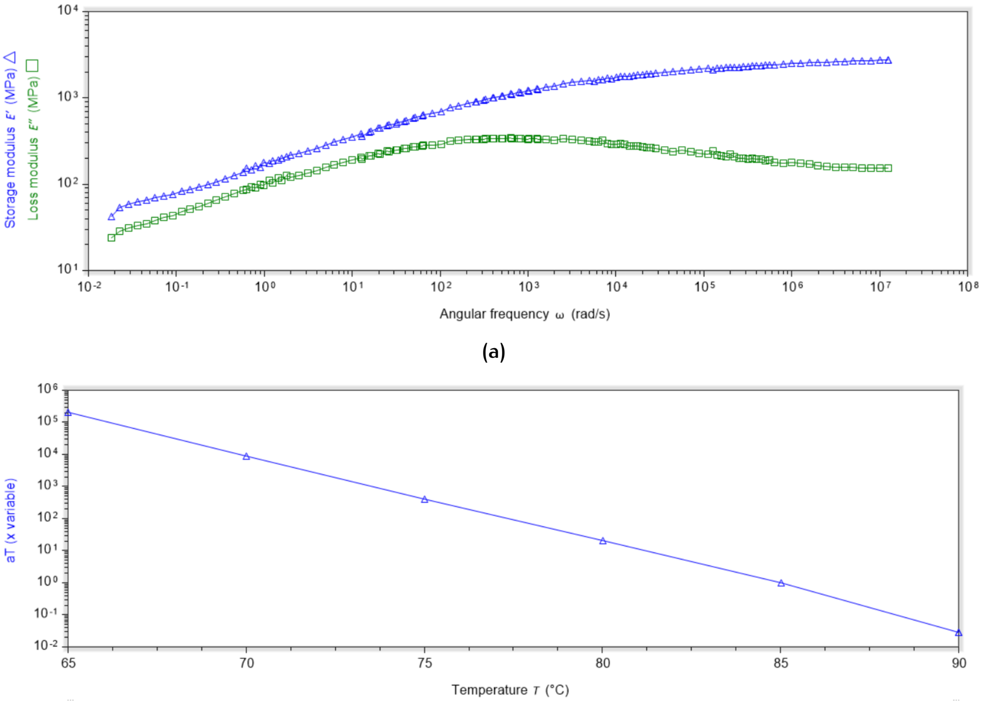

(a)

(b)

Figure A.12: Reduced TTS master curve and horizontal shift factors aT for: B1 (pristine state). Tref = 85°C

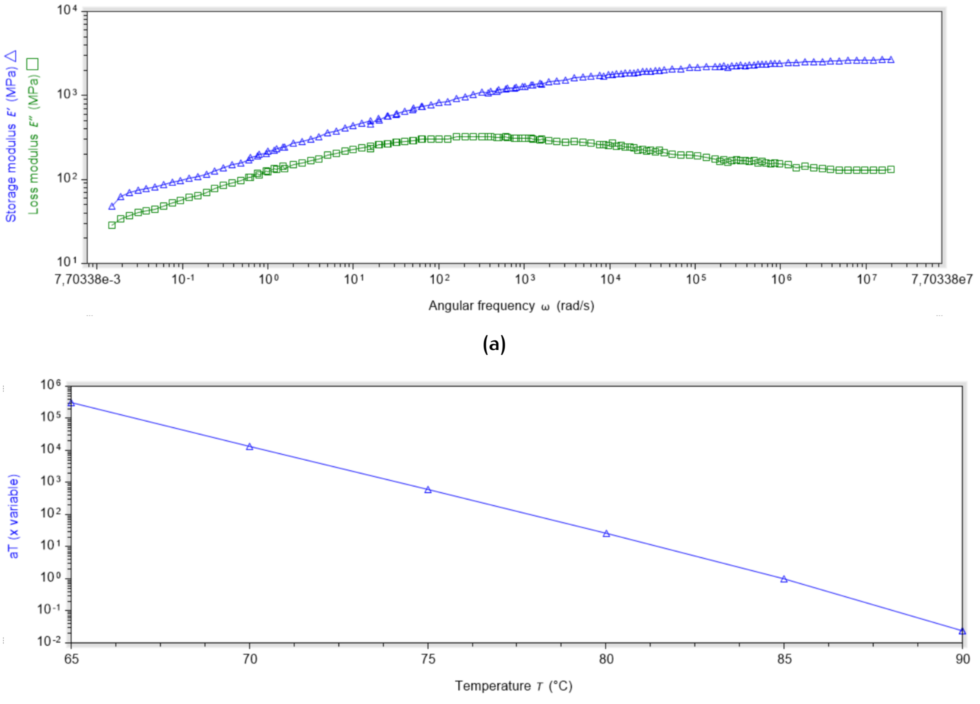

(a)

(b)

Figure A.13: Reduced TTS master curve and horizontal shift factors aT for: B2 (pristine state). Tref = 85°C

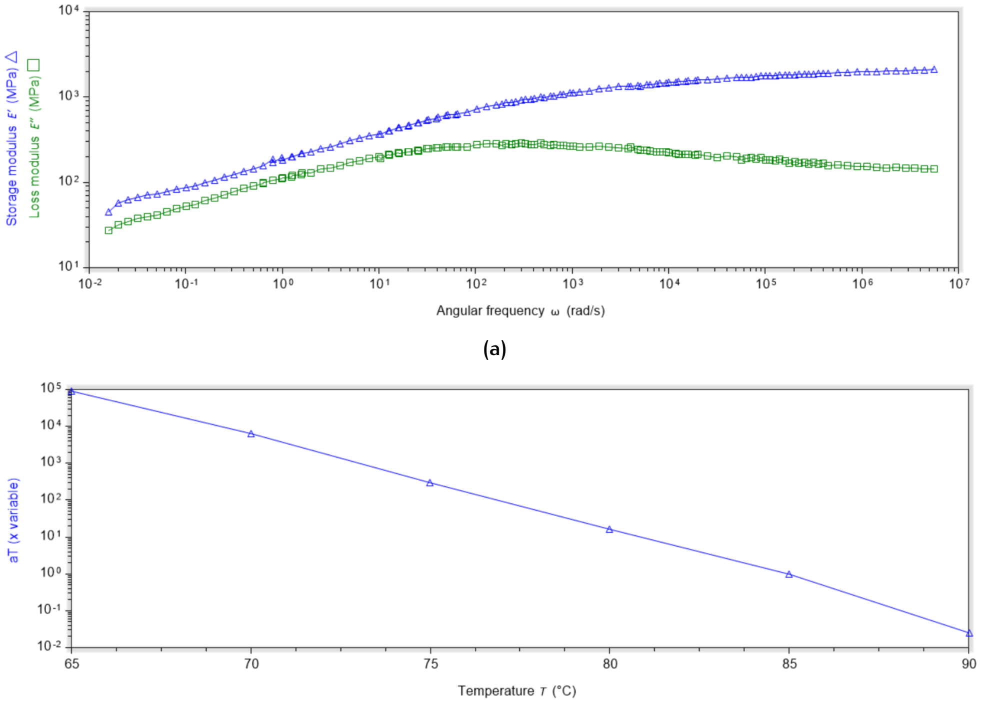

(a)

(b)

Figure A.14: Reduced TTS master curve and horizontal shift factors aT for: B3 (pristine state). Tref = 85°C

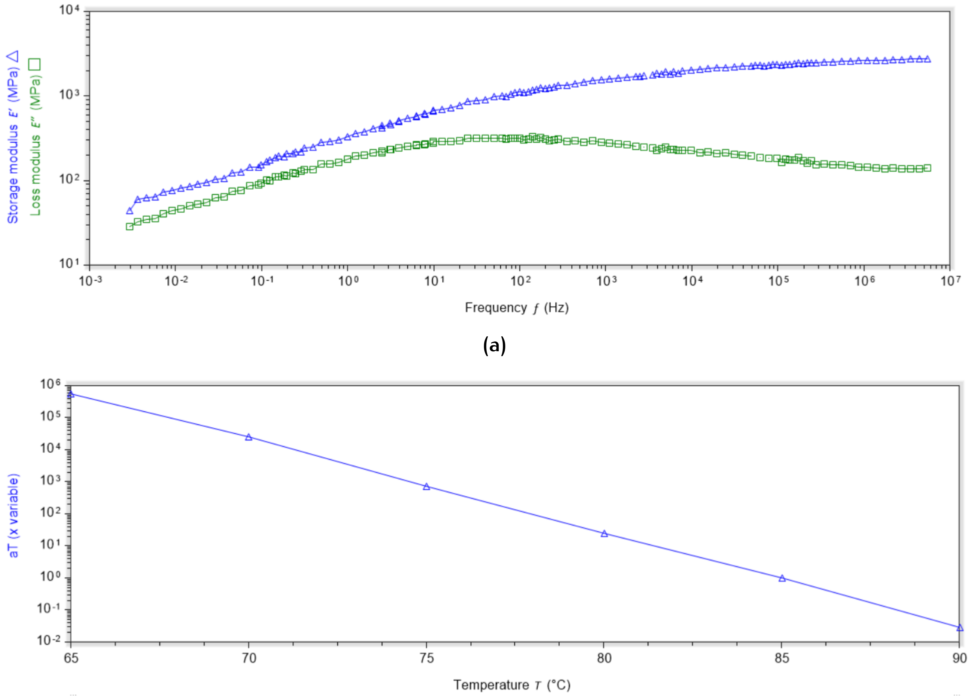

(a)

(b)

Figure A.15: Reduced TTS master curve and horizontal shift factors aT for: A1-m (damaged state, 10 minutes of recovery time). Tref = 85°C

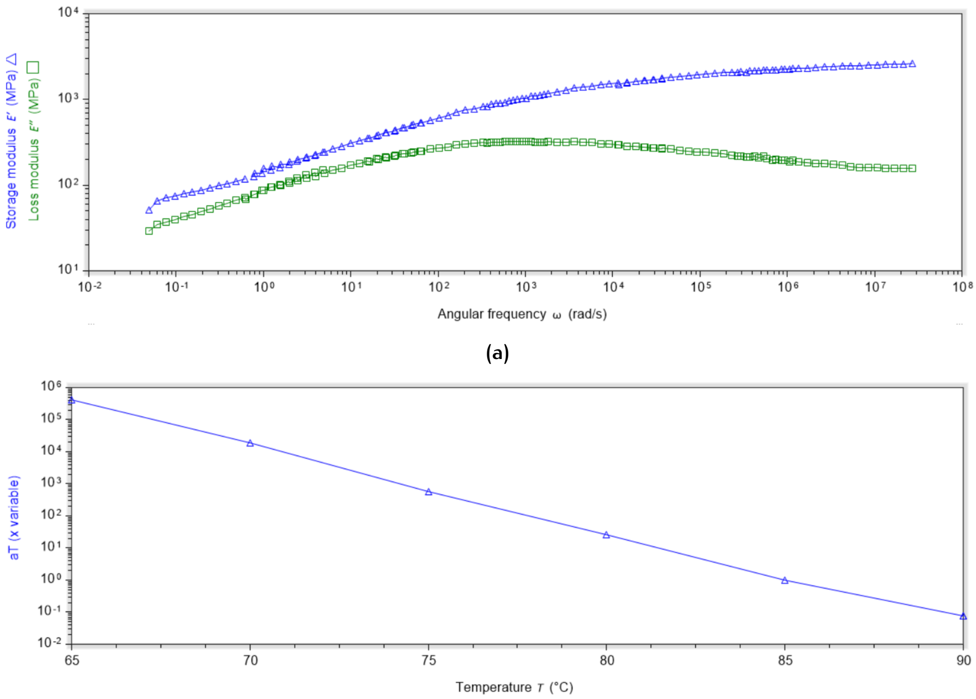

(a)

(b)

Figure A.16: Reduced TTS master curve and horizontal shift factors aT for: B1-m (damaged state, 10 minutes of recovery time). Tref = 85°C

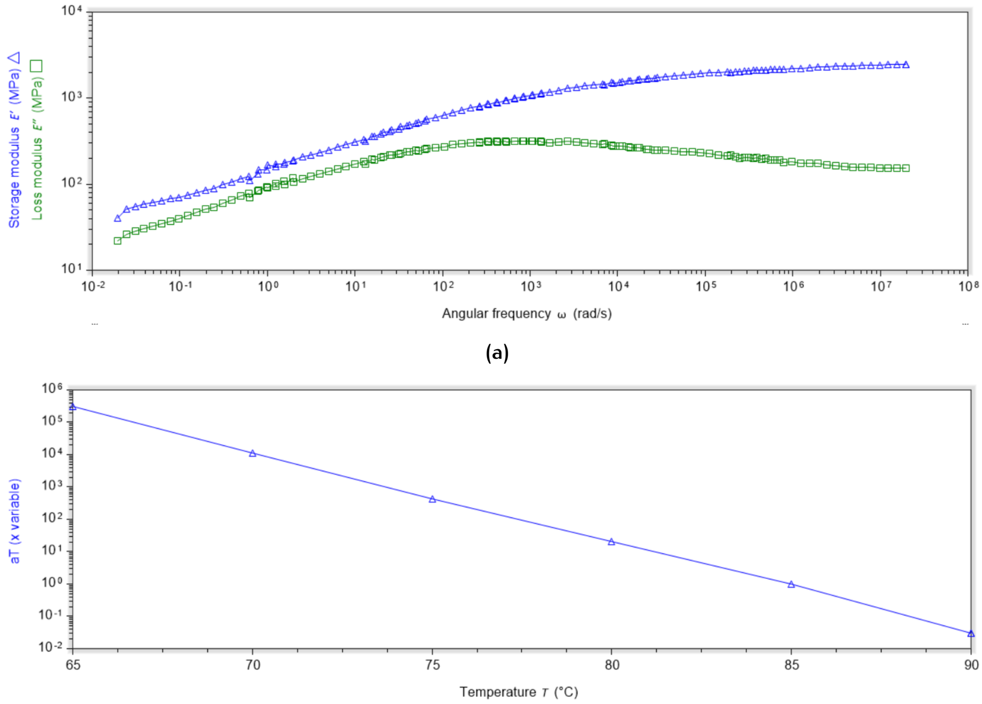

(a)

(b)

Figure A.17: Reduced TTS master curve and horizontal shift factors aT for: B2-m (damaged state, 10 minutes of recovery time). Tref = 85°C

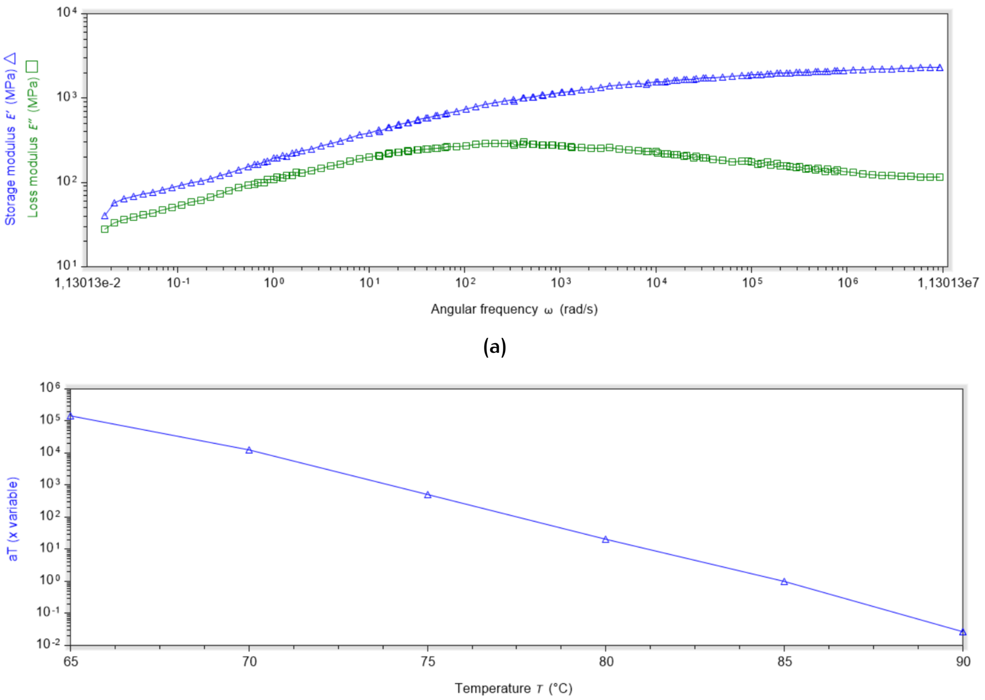

(a)

(b)

Figure A.18: Reduced TTS master curve and horizontal shift factors aT for: A1-w (damaged state, 1 week of recovery time). Tref = 85°C

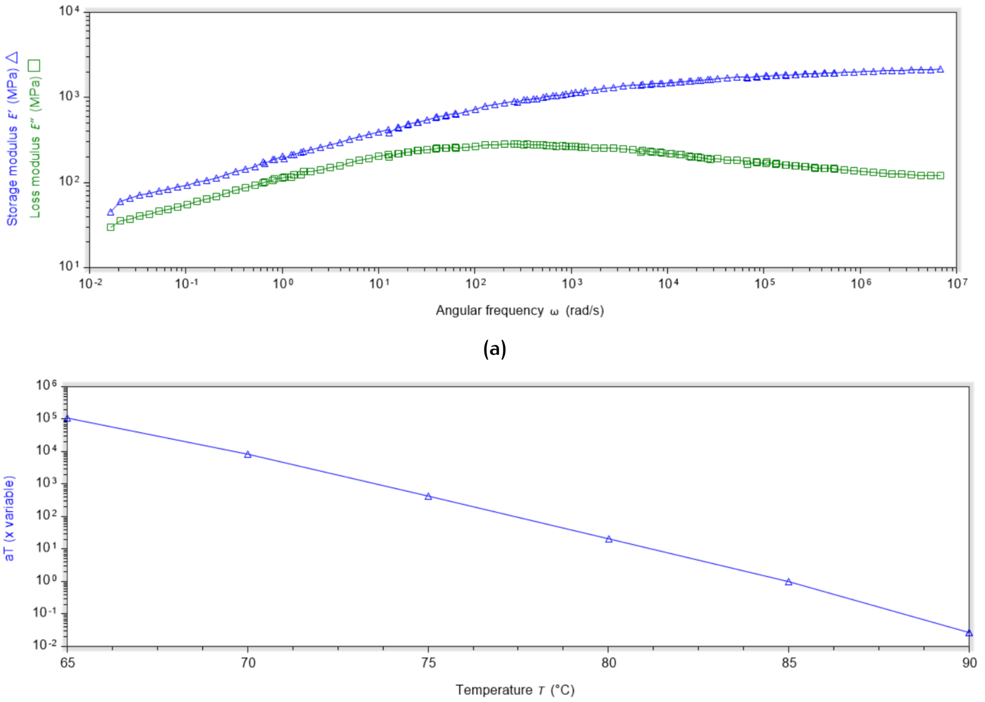

(a)

(b)

Figure A.19: Reduced TTS master curve and horizontal shift factors aT for: A2-w (damaged state, 1 week of recovery time). Tref = 85°C

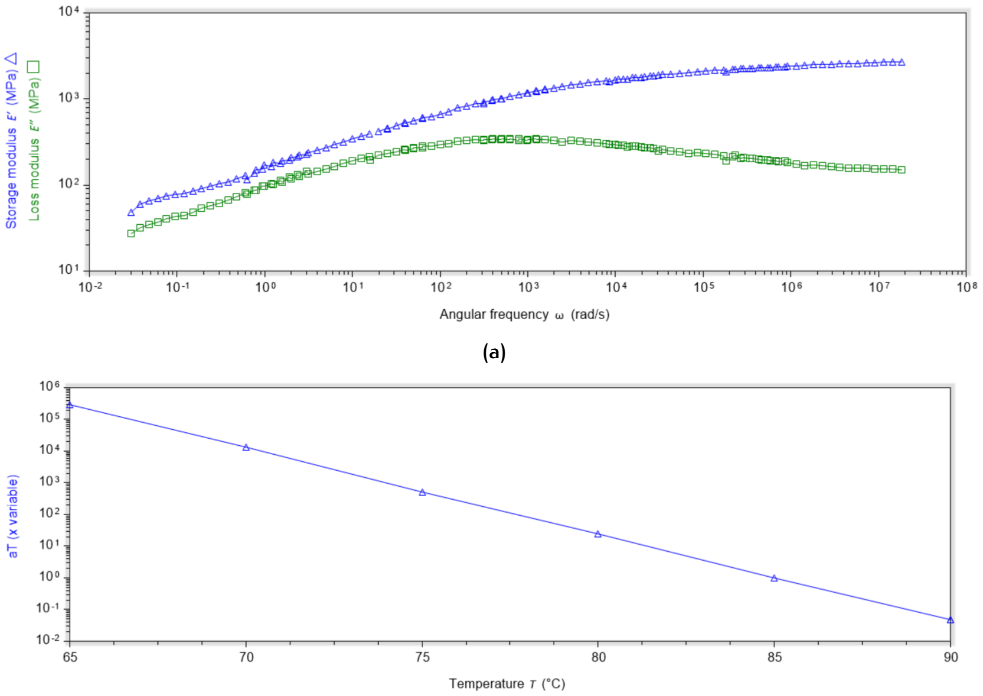

(a)

(b)

Figure A.20: Reduced TTS master curve and horizontal shift factors aT for: B1-w (damaged state, 1 week of recovery time). Tref = 85°C

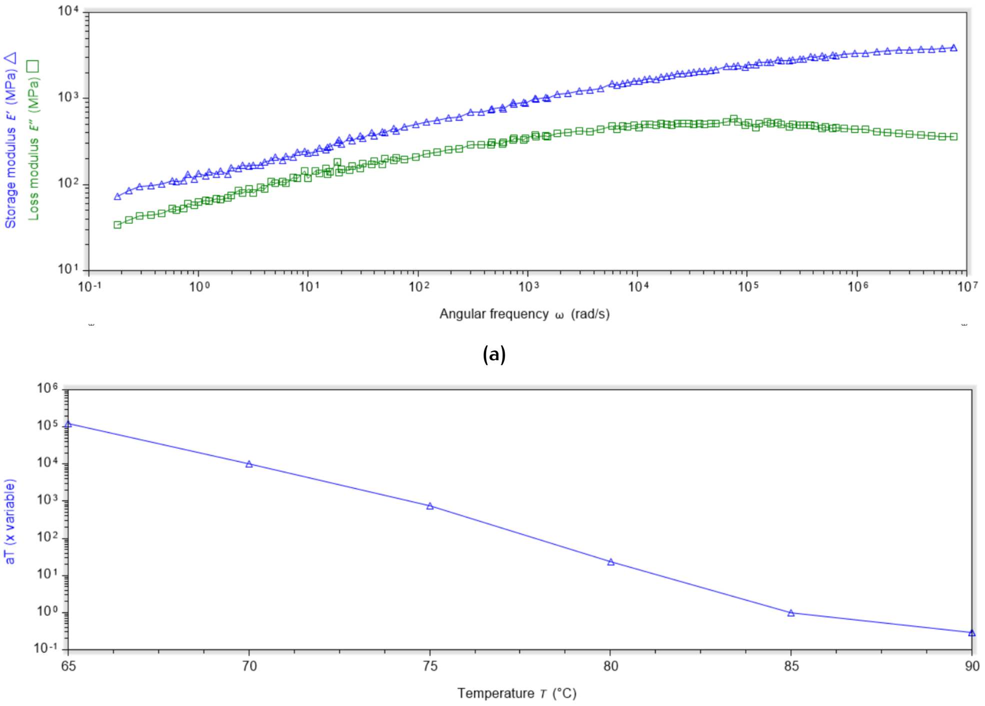

(a)

(b)

Figure A.21: Reduced TTS master curve and horizontal shift factors aT for: B-s (pristine state, after oven). Tref = 85°C

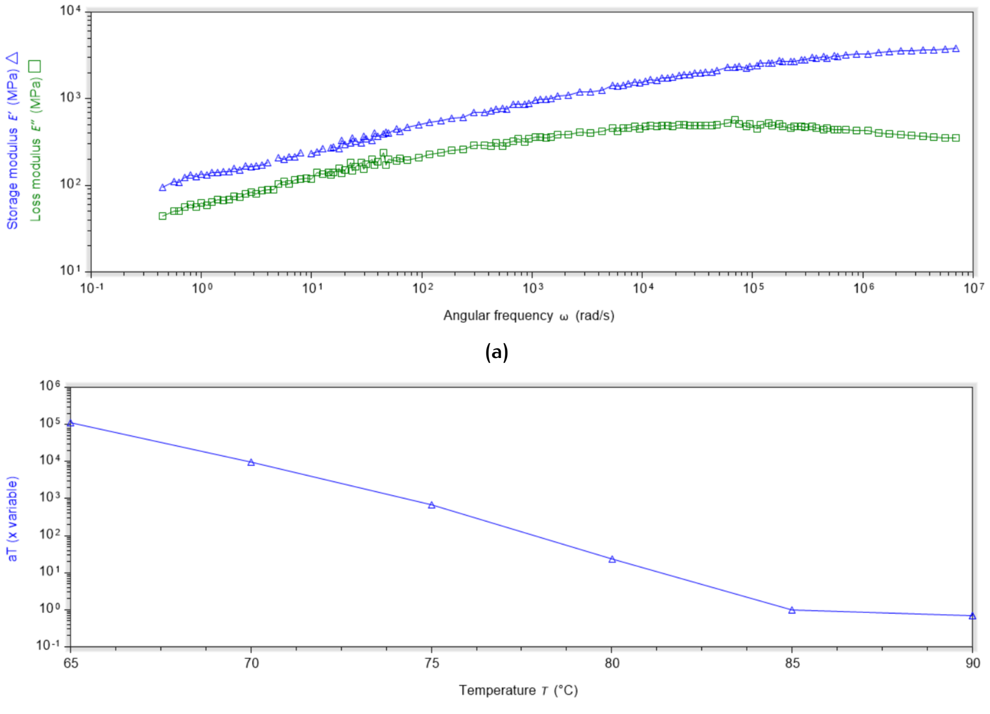

(a)

(b)

Figure A.22: Reduced TTS master curve and horizontal shift factors aT for: B-Ds (damaged state, after oven). Tref = 85°C

COLOPHON

This document was typeset using LaTeX. The document layout was generated using the arsclassica package by Lorenzo Pantieri, which is an adaption of the original classicthesis package from André Miede.